Bachelorarbeit

Zur Erlangung des akademischen Grades Bachelor of Science

Using Landsat time series for mapping winter and spring crops in Southeastern Anatolia

eingereicht von:

Gutachter: Prof. Dr. Patrick Hostert

                      Dr. Dirk Pflugmacher

                      M.Sc. Philippe Rufin (Betreuer)

Eingereicht am Geographischen Institut der Humboldt-Universität zu Berlin am:

Abstract

It is crucial to monitor land use intensity of cropland in order to better understand the land and water resource demands of agricultural systems. Remote sensing can improve the understanding of spatial and temporal variabilities of cropland systems through the analyses of time series. The Southeastern Anatolia Project (GAP), located in the semi-arid Euphrates-Tigris Basin, is Turkey's largest and most expensive regional development program, aimed to store and distribute water from the Euphrates and Tigris rivers for the irrigation of arable land. To estimate how winter and spring crops are spatially distributed in the GAP, this study used 140 atmospherically corrected and topographically normalized Landsat Collection 1 Tier 1 images across 12 WRS-2 footprints in 2015, to compute a quarterly composite and spectral-temporal metrics. To map winter and spring crops, training data was collected and with spectral-temporal variability metrics applied to a non-parametric classifier for the three-month composite from 1st April until 26th June 2015. Area-adjusted accuracies were calculated to assess map accuracy, area and 95% confidence intervals. The results showed a satisfactory separation of land cover, reaching an overall accuracy of 83.71 (± 2.31%), producer's accuracy of 89.23% (± 4.13%) and user's accuracy of 97.58% (± 2.35%) for the winter and spring crops class. Cropland area-adjusted calculations revealed a total expanse of winter and spring crops of 1,737,355 hectares (± 88,639 ha) of land in 2015, which is equal to 22.2% (± 1.13%) of the study area. However, the relatively high error of omission (10.77%) proposes an underestimation of the winter and spring crops class due to the confusion with the grassland class. Province-level statistics detected the absolute largest expansions of winter and spring crops in Diyarbakır (415,739 ha) and Şanlıurfa (431,525 ha), while the highest proportion (>80%) of winter and spring crops on agricultural land is found in the provinces of Kilis, Adıyaman, Diyarbakır, Batman and Siirt. The approach could be transferred to create annual change maps for winter and spring crops, assuming sufficient data availability.

Table of Contents

List of Figures

List of Tables

1. Introduction

Agricultural expansion and intensification have made it possible to feed an ever faster growing number of people on this planet. Climate variability and population growth are exerting increasing pressure on the agricultural land and its water use (Fritz et al., 2015). Due to population growth, which is expected to reach 9.8 billion people in 2050 (UN, 2017), worldwide demand for crops is predicted to grow by more than 100% between 2005 and 2050 (Tilman et al., 2011). While the rate of agricultural expansion has slowed globally, the intensification of land use is leading to higher yields. The Green Revolution in the middle of the 20th century has accelerated the process of intensification, especially in developing countries (Ramankutty et al., 2018). The main reasons for increasing harvest output lie in the rising frequency of global cultivation through additional cropping cycles (Ray and Foley, 2013) and in the enhanced input intensity using water, fertilizer and pesticides (Erb et al., 2013; Foley et al., 2011). However, agricultural expansion and intensification threatens biodiversity (Zabel et al., 2019) and is a major cause of environmental degradation (Ramankutty et al., 2018).

Agriculture is the sector with the highest water consumption worldwide (Siebert et al., 2013) and global agricultural production depends on irrigation, especially in water scarce regions and during periods of insufficient rainfall (Johansson et al., 2016). Under changing climate, rising CO_2 levels and population growth, the water availability per person is likely to decrease in many regions (Gerten et al., 2011). Furthermore, excessive irrigation practices could ultimately raise the risks of water scarcity and soil salinization (Mekonnen and Hoekstra, 2016) and could increase conflicts and tensions over freshwater resources (Johansson et al., 2016). Some studies conclude that irrigated arable land should be converted into rain-fed management in the future, as irrigation is not suitable to compensate for varying climatic influences due to freshwater shortages and population growth (Elliott et al., 2014). In order to meet the future needs of food production, a more sustainable management of land use and water consumption is unavoidable. In most parts of the world, it is also no longer feasible to expand cultivated land (Porkka et al., 2016). Ray et al. (2019) further showed, that climate change has already affected global crop production.

In order to improve the monitoring of current and future land and water resource needs, it is necessary to map spatially consistent cropping practices on a larger scale and beyond the regional level (Jägermeyr et al., 2015). Current knowledge of these processes is scarce (Ray and Foley, 2013), and statistics on the intensity of land use may underlie potential bias. Since the need for knowledge of regional agricultural practices is expected to increase (Bégué et al.,

2018), remote sensing can improve the understanding of spatial-temporal variabilities of cropland systems across administrative borders (Deines et al., 2017). In particular Landsat-based medium resolution data analyses have shown that they offer the capability to map the extent of cropland over large areas using spectral-temporal variability metrics. These variability metrics have shown to be a robust predictor of land cover by capturing seasonal variations of land surface spectra (Dong et al., 2016; Song et al., 2017; Rufin et al., 2018; Müller at al., 2015; Pflugmacher et al., 2019). The opening of the Landsat image archive in 2008 (Woodcock et al., 2008), combined with the use of Google Earth Engine, a cloud-based platform for planetary geospatial analysis (Gorelick et al., 2017), allows large-scale analysis of image time series at 30 m spatial resolution (Wulder et al., 2012).

Around one third of Turkey's land area is being cultivated (FAO, 2009) and the Euphrates-Tigris Basin in Iraq and Turkey is an area of high irrigation density of regional importance (Siebert et al., 2013). With an area of 0.7 million hectares, Turkey has the fifth largest extension of reservoir-irrigated croplands in the world (Rufin et al., 2018), and 71.3% of Turkey's farmland was cultivated in winter and spring in 2015 (Rufin et al., 2019). Intensive cultivation patterns are observed in the Şanlıurfa and Mardin provinces of the Southeastern Anatolia Project (GAP), with a high share of double, summer, winter and spring cropping practices (Rufin et al., 2019). The GAP is Turkey's largest and most expensive regional development program, covering 9 Turkish provinces. The main objective of the GAP, located in the semi-arid Euphrates-Tigris basin and the plain of upper Mesopotamia, was to store and distribute water from the Euphrates and Tigris to contribute to economic and social development (GAP, 2019a).

A recent study investigated the extent and frequency of irrigated summer cropping in the GAP region (Rufin et al., in prep.). In the study summer-cropped areas were mapped as a proxy for irrigation in the region and the total irrigated area was likely underestimated, as irrigated winter crops were not included. However, a high share of winter and spring crop practices are also prevalent in the study area (Rufin et al., 2019). Spring and winter cropping, which cover extensive areas of winter cereals that are also irrigated but with relatively low water requirements, dominate in Turkey (Rufin et al., 2019; Lopes et al., 2018).

In arid regions, the growing cycles of cultivated lands are largely dependent on precipitation. However, irrigation locally decouples the cultivation of cropland from rainfall-related restrictions on water availability, making it difficult to judge whether winter and spring crops are rain-fed or irrigated. Most rainfall occurs between November and April which increases the

likelihood that they will be precipitation-driven in winter and early spring, but irrigated during spring (Özdoğan et al., 2006).

In winter and spring, problems such as reduced data availability due to cloud contamination are overcome (Kovalskyy and Roy, 2015) by using all available Landsat 7 and -8 data to calculate a quarterly composite and spectral-temporal metrics. Spectral-temporal metrics help to differentiate between heterogeneous land cover, since it reduces the impact of clouds and cloud-shadows (Pflugmacher et al., 2019). By combining spectral temporal variability metrics and quarterly composites, classification accuracies are considered to improve (Rufin et al., 2019). Furthermore, the derivation of these features has proven to be consistent over multiple time periods and large areas (Waldner at al., 2017), and various case studies have shown their advantages for mapping cropping practices (Oliphant et al., 2019; Phalke & Özdoğan, 2018). Using a quarterly time window provides a good trade-off between temporal detail to capture the maturity stage of winter and spring crops and observation availability (Rufin et al., 2019).

The aim of this study is to assess the distribution of winter and spring cropping in order to understand the different cropping practices of irrigated and rain-fed agriculture in the GAP using Landsat time series and spectral-temporal variability metrics.

Concretely, the study intends to answer the following research question:

Which three-month time window has the best data availability in the GAP region in 2015 (i) to map and validate winter and spring crops (ii) and to what degree do they overlap with irrigated summer crops (iii)?

The specific objectives being investigated within this study:

  i. Identification of the best quarterly time window between beginning of March and end of July in 2015
 ii. Mapping and validation of winter and spring crops in 2015
iii. Analyses of the degree of overlap of winter and spring crops and irrigated summer crops in 2015 to identify region-specific characteristics at the province-level within the GAP

2. Study Area

The Southeastern Anatolia Project (Güneydoğu Anadolu Projesi)

The Southeastern Anatolia Project, bordering Syria to the south and Iraq to the southeast, is located in Turkish Southeastern Anatolia and comprises nine provinces (Figure 1). The GAP is the largest and most expensive regional development program of the Republic of Turkey. Its area extends over the Euphrates-Tigris Basin and the plains of upper Mesopotamia and was officially administrated in 1977 by the General Directorate of State Hydraulic Works (GAP, 2019b; Bilgen, 2018a).
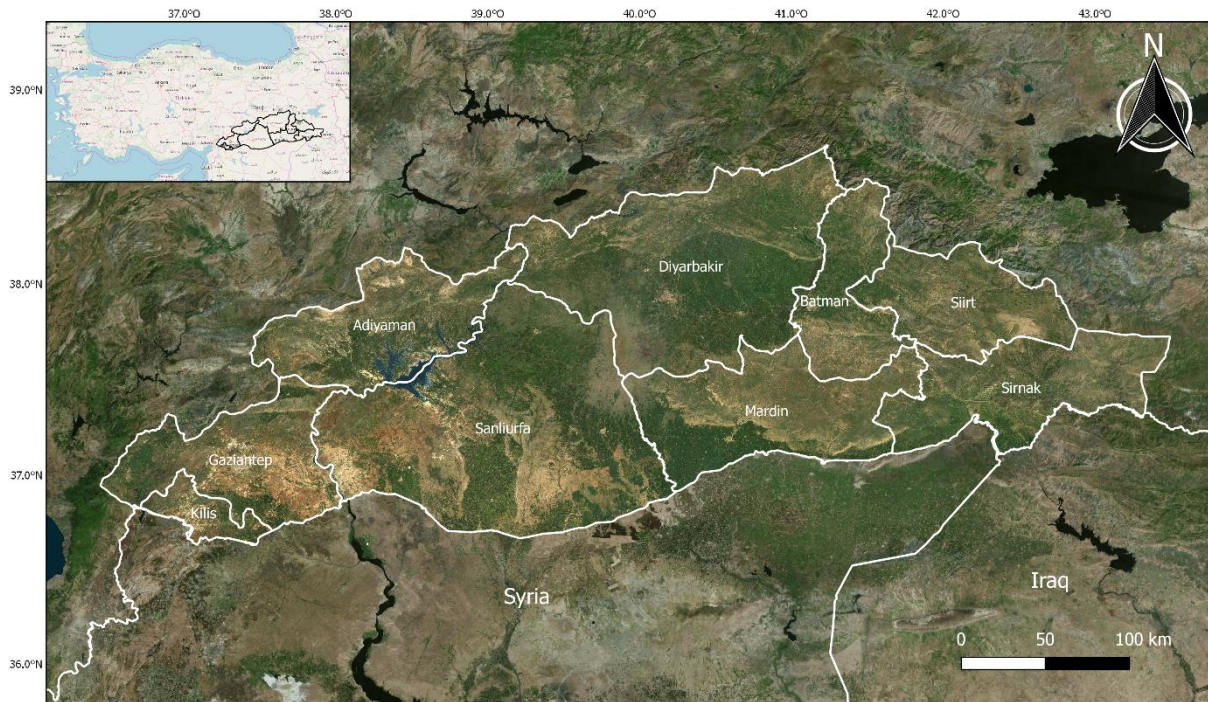
Figure 1. *True color satellite image (Greenest Pixel Composite from Landsat ETM+ and OLI data) of the nine provinces within the GAP region in Turkey representing March to July 2015.*

The region covers an area of 75,000 km^2 and on average, the GAP provinces account for 10.7% of Turkey, both geographically and in terms of population (GAP, 2019a). The GAP region accounts for more than half of the area Turkey's area planted with cotton and the Turkish government has spent more than US$ 25 billion over the past three decades (USDA, 2019). The GAP was launched in 1989 under the GAP Master Plan aiming to store and distribute water from the Euphrates and Tigris rivers to contribute to economic and social development by 2005 (Bilgen, 2018a). Originally the aim of the GAP master plan has been to bring 1.8 million hectares of land under irrigation by constructing 22 dams and 19 hydraulic power plants in total. However, in 2017 the project reached 545,938 hectares, which means only 30.3% of the irrigation projects is now in operation (GAP, 2019c). According to Rufin et al. (in prep.)

summer-cropped areas increased since 1990 by 617%, to a total of 577,887 hectares in 2018 while the United States Department of Agriculture estimates, that about 650,000 hectares of land is to be currently irrigated (USDA, 2019).

Several reasons are mentioned for the delay, but among the most important are the Turkish-Kurdish conflict, socio-environmental and historical-cultural concerns, and international geopolitical interests (Hommes et al. 2016). Nearly one-fifth of the total irrigable land and one-third of the energy potential of Turkey are in the region (Altinbilek and Tortajada, 2012). Since its official disclosure in the 70'ies, the GAP has evolved from a technical, state-run and mainly infrastructural and economic development project to a social, market-oriented and sustainable human development project due to numerous adjustments (Bilgen, 2018b). In recent years the economic downturn, including the depreciation of the Turkish Lira, and technical problems as well as security issues in the region are reportedly slowing down the progress (USDA, 2019).
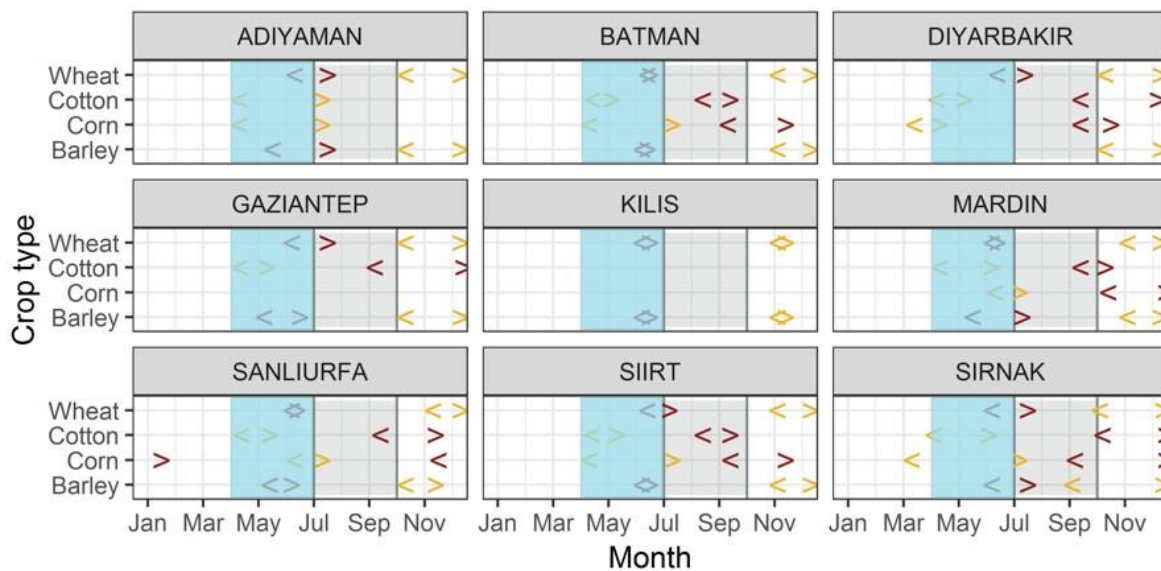
***Figure 2**. Regional crop calendar, indicating the start (<) and end (>) of the planting phase (yellow) as well as the start (<) and end (>) of the harvest period (red) for four major crops in the GAP region. Grey shading indicates the observation time window window defined in the comparative study of Rufin et al. (in prep.) mapping summer crops. Blue shading indicates the observation time window defined in Section 4. Data compiled by the Turkish Ministry of Agriculture and Forestry (TARIM, 2015). Planting and harvesting dates were not available for all crops and provinces. Figure derived following Rufin et al. (in prep.).*

Prior to the initiation of the GAP, the region was characterized by rainfed cultivation of winter and spring crops (Metin Sezen and Yasar, 2006). The main winter and spring crops are wheat and barley, while the major summer crops are cotton and corn (Figure 2). Figure 2 shows that winter and spring crops are planted in the previous year, reach their season peak between April and May and are harvested at the end of June (Rufin et al., 2019). Other winter and spring crops, such as predominantly rain-fed cereals, are usually harvested mid to late May (Özdoğan et al., 2006).

Climate

The GAP is located in one of the most arid regions in Turkey, due to a high rate of evaporation and low rate of rainfall (Bilgen, 2018a). The semi-arid climate is characterized by precipitation between 200 and 600 mm/year, but with little to near-zero precipitation during summer and a high rate of evaporation which frequently exceeds 2,000 mm/year (FAO, 2009). Following Köppen-Geiger Climate Classification, most of the study area is located within the warm temperate climate with dry summer. Precipitation only appears during winter whereas the temperature is hot during summer. The monthly mean temperature of the coldest month is above -3 °C but less than +18 °C and the monthly mean temperature of the warmest month is equal to or greater 22 °C (Kottek et al., 2006).

Exceptions are the region around Harran in Şanlıurfa and eastern parts of Şırnak as well as parts of the north of both Diyarbakır and Batman. In southern Şanlıurfa there is arid steppe climate with annual mean near-surface temperature equal to or greater than 18 °C and accumulated annual precipitation greater than 360 mm/year, with at least two third of the annual precipitation occurring in winter. The eastern parts Şırnak and the northern parts of Diyarbakır and Batman are snow climates with dry summer which predominate in more highly situated regions. At least four months are above the 10 °C average, while the coldest month is below the 0 °C or -3 °C average (Kottek et al., 2006).

The Euphrates with 2700 km and the Tigris with 1900 km are the rivers with the highest water content in the Near East. The areas from the headwaters to the estuaries of the two rivers are very different in topography and climate. Both originate in the eastern Anatolian highlands with elevations of more than 3000 m and high precipitation, which amount to 785 mm at the Tigris and 585 mm at the Euphrates in the catchment area of the river headwaters in the long-time middle mean. To the south and southeast, precipitation quickly decreases to below 100 mm per year and the arid season becomes longer respectively. If the resources of the drainage area of both rivers are combined, the water-basin members have a total of 84 billion cubic meters of water at their disposal each year. 88.8% of the total Euphrates water and 51.9% of the Tigris water, respectively 67.4% of the total water potential of the Greater region, are generated on Turkish territory. The natural runoff behavior of both streams is extremely unfavorable for use by the residents. In the eastern Anatolian mountains, the high winter precipitation is largely stored as ice and snow. With the melting snow and the spring precipitation, the amount of water increases very rapidly until April (Glaser and Kremb, 2013).

3. Data and Methods

One objective of this study is to compare the results with those of Rufin et al. (in prep.), hence 2015 was chosen as target year for better comparability. In addition, this year has shown good data availability with high-resolution imagery available in Google Earth. The methods of this study are similar to the comparative study (Rufin et al., in prep.). For mapping winter and spring crops in the GAP, however, it was first analyzed which quarterly time window during the growth phase in 2015 has at least three valid observations per pixel, which are not compromised by cloud, cloud-shadow and snow. Training data were then collected, and spectral-temporal variability metrics were computed. The training data and the spectral-temporal variability metrics were applied to a non-parametric Random Forest classifier (Breiman, 2001) for the three-month composite in 2015. Subsequently, the expansion of winter and spring crops was mapped and validated. Finally, the binary winter and spring crops classification was compared with irrigated summer crops (Rufin et al., in prep.) to identify areas which undergo two growth cycles on province-level in 2015.

Landsat time series (Data & Pre-Processing)

Since the change of the Landsat archive data policy by the joint program of the U.S. Geological Survey (USGS) and the NASA in 2008, the access to Landsat imagery is made freely available to all users via the internet. One of the oldest Earth-observing satellite programs spans more than four decades with a spatial resolution of 30 meters and enables the analysis of changes in Earth's surface back to 1972 (Woodcock et al., 2008). The opening of the Landsat data archive has advanced the monitoring and modelling of the terrestrial land cover and ecological change over time and across large areas. As a result of its global coverage, the archive provides uniform methods and applications that ultimately improve scientific and environmental monitoring products (Wulder et al., 2012; Wulder and Coops, 2014).

Since the study area covers approximately 75,000 km^2 and therefore requires a lot of computing power, Google Earth Engine was used to access and pre-process data as well as to perform the classification. Google's massive computational capabilities, accessed and controlled via an Internet-accessible application programming interface (API) and a web-based interactive development environment (IDE), allow large-scale satellite-based analyses and visualization of geospatial data sets. These services are free to use for research, education, and non-profit purposes (Gorelick et al., 2017). By the expansion of parallel processing and Googles cloud-computing centers, it is now even feasible to create globally consistent and locally relevant maps, as several case studies show (Hansen et al., 2013; Pekel et al., 2016).

All available Landsat 7 (ETM+) and Landsat 8 (OLI/TIRS) Surface Reflectance data were used. After the USGS reorganized the Landsat archive into a tiered collection in 2016 (USGS, 2019a), the Landsat Level-1 products provide a consistent archive of known data quality to support time-series analyses and data stacking (USGS, 2019b). The data in Tier 1 meet formal geometric and radiometric quality criteria. It includes Level-1 Precision and Terrain (L1TP) corrected data that have been radiometrically calibrated and orthorectified using ground control points and digital elevation model (DEM) data to correct for relief displacement. The Landsat Collection 1 Surface Reflectance product (L1TP Tier 1) is the highest quality Level-1 product suitable for pixel-level time series analysis (USGS, 2019b) and therefore ensures radiometric and geometric consistency between input data from different Landsat sensors, footprints, and acquisition data. Both satellite datasets are strips of collected data and are packaged into overlapping scenes covering approximately 180 km x 185 km using a standardized reference grid (USGS, 2019a).

The atmospherically corrected surface reflectance datasets from the two sensors are using different algorithms. The Landsat 7 Surface Reflectance product is atmospherically corrected from Enhanced Thematic Mapper Plus (ETM+) sensor using LEDAPS algorithm (Schmidt et al., 2013; USGS 2019c), while the Landsat 8 Surface Reflectance dataset is the atmospherically corrected surface reflectance from the Landsat 8 Operational Land Imager (OLI) and the Thermal InfraRed Sensors (TIRS) using LaSRC algorithm (USGS 2019d). Both products include a cloud, shadow, water and snow mask produced using CFMASK algorithm (Foga et al., 2017; USGS 2019e), as well as a per-pixel saturation mask, with the results represented as bit-mapped values within the Landsat Collection 1 Level-1 Quality Assessment (QA) Band (USGS, 2019f; Zhu et al., 2015).

The spectral resolution of Landsat is defined by its bands. For merging Landsat 7 and Landsat 8, only three visible (Blue, Green, Red), one near infrared (NIR) and two shortwave infrared (SWIR) bands of the Landsat 8 OLI sensor (USGS, 2019g) and the Landsat 7 ETM+ sensor (USGS, 2019h) were used, all with a 30 m spatial resolution. The ultra-blue band of Landsat 8 is not used and the panchromatic bands (ETM+ Band 7, OLI Band 8) are not processed to surface reflectance but are required as input in order to generate the accompanying cloud mask (Google Developers, 2019).

Data availability

The strong spatio-temporal variability of the phenology of arable land and the irregular acquisition of cloud-free images for optical data, especially in the winter period with increased

cloud coverage, pose a challenge to the robust mapping of annual cultivation practices (Whitcraft et al., 2015). Considering the relatively long revisit time of the Landsat sensor family (16 days in nadir) and higher cloud coverage in winter, Landsat might only provide few unclouded scenes per growing season, which lead to an irregular observation density (Ju & Roy, 2008). This is aggravated by sensor related errors, like the failure of the Scan Line Correction in May 2003 (Markham et al., 2006).

Due to Landsat revisit interval of 16 days, there are approximately 6 acquisitions per satellite over a three-month period. If the scenes overlap, then there are more, so each pixel on the map is derived from a stack of pixels. In addition, the Landsat sensor family has two satellites in operation in 2015 and repeat coverage can then be up to eight days, resulting in higher revisit frequency, especially in the across-track overlap areas (Kovalskyy and Roy, 2013). All available Landsat 7 and -8 images were used, but due to different cloud, cloud shadow and snow coverage these pixels may be of no use for further analyses and are therefore masked and excluded from the analysis. To assess whether a pixel is suitable or not, the band containing attributes generated from the CFMASK algorithm (pixel_qa) is extracted and only valid pixels (after snow, cloud and cloud shadow masking) are used and others are excluded (USGS, 2019f; Zhu et al., 2015).

To meet winter and spring crop maturity stage, a time window between the start of the green-up in 2014 and harvest at the end of June is targeted (Rufin et al., 2019). A quarterly time window for compositing is considered appropriate as a trade-off between temporal detail and observation availability to compute spectral-temporal metrics (Rufin et al., 2019). The aim is to find a suitable three-month time window in 2015 to have at least three valid observations per pixel at hand for the classification.

The computed valid pixel count for the determined time windows includes all areas that are free of clouds, cloud shadows and snow and that were not compromised by radiometric saturation, after Rufin et al. (2019), hereinafter referred to as clear sky-observations (CSO). The CSOs were calculated by adding a date band to each image in the collection to count all valid observation pixel, neglecting WRS-row overlap. The aim is to find at least three CSOs per pixel. Therefore, a total of five quarterly time windows were investigated, by downloading the CSO raster and computing frequencies in R (The R Project, 2015). The first quarter of 2015 is considered to contain too few usable images and the period after the end of July already contains summer crops (Figure 2, p. 10). The earliest time window investigated began at the beginning of March and the other windows follow at two-week intervals. The last window ended at the

end of July. In addition to the pixel-based CSO count analyses, the image count and the average cloud cover for the five time windows considered were derived.

Spectral-temporal metrics

After a suitable three-month time window was found, spectral-temporal metrics were derived. Combining spectral temporal variability metrics and quarterly composites, classification accuracies are expected to improve (Rufin et al., 2019). The deviation of spectral-temporal variability metrics has proven to be consistent over multiple time periods and large areas (Waldner at al., 2017), and the use in various case studies implied their advantages for mapping agricultural land (Oliphant et al., 2019; Phalke & Özdoğan, 2018). They can provide temporally consistent means for cropland mapping (Rufin et al., in prep.; Schmidt et al., 2016; Deines et al., 2017), since they contain information on land surface phenology, which makes them suitable for mapping cultivation practices across gradients of climate, topography or land use intensity (Ambika, Wardlow, & Mishra, 2016). Furthermore, they can eliminate the strong limitations of cloud coverage through image-based classification methods, thereby reducing the effects of cloud and cloud shadow (Pflugmacher et al., 2019). Thus, seven spectral-temporal metrics, that capture the distribution and variability of reflectance, were used to distinguish winter and spring crops from other land cover classes in the GAP region. Median, mean, minimum, maximum, 25th and 75th percentile spectral reflectance plus standard deviation of all reflectance values were calculated. To include all spectral information, the seven metrics were calculated for each of the six spectral bands individually (blue, green, red, near infrared, and two shortwave infrared bands) of Landsat 7 and Landsat 8 at the pixel level, resulting in a total of 42 spectral-temporal features for the identified three-month time window. Including the red edge (R – NiR) in the analysis, the accuracies are expected to improve (Griffiths, Nendel & Hostert, 2019), also since the combination of mean and standard deviation should support distinguishing cropland, pasture and natural savanna vegetation (Müller et al., 2015).

Training Data (Class Catalogue) & Classification

The study area consists of four ecoregions within the Palearctic realm. The eastern Mediterranean conifer-broadleaf forests ecoregion, the eastern Anatolian deciduous forests ecoregion, the Zagros Mountains forest steppe and the eastern Anatolia montane steppe (Dinerstein et al., 2017; WWF, 2019). Since they consist of heterogenous land cover (forests, woodland, shrubs, grassland, savannas, shrublands, urban, water), a class catalogue consisting of winter and spring crops and five other land cover classes was chosen for training data collection. Other classes included water, grassland, built-up areas and open soil, forested areas

and other arable land (Table 1, p.16). The winter and spring crops class includes areas of clearly visible vegetative activity during the season peak around April and May. These are recognizable by the steep red edge (Seager et al., 2005) and the alteration to a less vegetative active phase after harvest. For this reason, the phenological differences, which are recognizable by the changing spectral signature between the maturity stage and harvest, were used as distinct signs of a winter or spring crop. The training points were classified on a pixel level (30 m x 30 m) using compositing and very high-resolution imagery available in Google Earth. Google Earth was used to identify agricultural areas and the other land cover classes, but in order to distinguish winter and spring crops from other arable lands, two further Landsat composites were used and displayed in false-color. One containing the green peak (two-month mean composite for April to May) and one after the harvest (two-month mean composite for June to July). As assistance, the spectral signatures of every training pixel was studied by using the Identify Features Function, implemented in QGIS (QGIS Development Team, 2019). This specific sampling class design guarantees that all surface types are included and that there is little to no overlap between classes so that there is a thematic unambiguity. To cover the heterogeneous land surface of the GAP, in total, 553 training points across the nine provinces were collected, of which 23% (128 samples) represented winter and spring crops (Table 1). However, this class could also include double cropping practices, which has two growing cycles and harvests within 2015, as a result including both winter and spring crops and summer crops at the same time (Rufin et al., 2019).

Table 1. Description of the Class catalogue following Rufin et al. (2019).

Classes (ID)	Description	Number of collected training points
Water (1)	Water bodies like natural lakes, rivers, reservoirs, water courses.	50
Winter and spring crops (2)	Green-up in 2014, season peak around April/ May 2015, followed by harvest at end of June 2015. This class also includes double cropping.	128
Grassland (3)	Semi-natural and managed grasslands, natural grassland, heathland, shrubland, but also pasture, and surfaces with little to much vegetation, scrubs and/or herbaceous vegetation, Transitional woodland-shrub with an open canopy.	119
Built-up/ open soil (4)	Built-up areas or artificial surfaces, infrastructure such as roads, dams, as well as urban and other sealing areas, open soil with little or no vegetation and without distinct phenology, bare rocks, sand, sparsely vegetated areas.	73
Forested (5)	Includes deciduous, evergreen and mixed forest.	75
Other arable land (6)	Olive groves, fruit trees and berry plantations, vineyards, irrigated summer crops, winter fallowed areas.	108

To convert quantitative spectral information into categorized land cover classes, a Random Forest classification algorithm was used (Breiman, 2001). To get the values for all samples in the training set, all seven spectral-temporal metrics were computed for the six bands of the

merged image collection and stacked into one image. This image stack, containing the quarterly composite and the spectral-temporal metrics, was afterwards used to train the classifier. To classify each feature in the collection, the Random Forest algorithm used n = 250 decision trees, the number of decision trees to create per class, and the square root of the number of variables per split. After the Random Forest model was applied, the classified image was downloaded and converted into a binary classification (winter and spring crops/ other) by selecting the specified class ID (Table 1, p.16).

Estimating accuracy, area and confidence intervals

Due to limited access to resources and the difficulty to visit the study area and compile ground truth data, the classification accuracy and class area extent was estimated (Olofsson et al., 2014). Following Cochran (1977), the reference sample size of n = 900 was estimated by specifying a target standard error for an overall accuracy of 1% and by conjecturing that user's accuracy will be 90% for all classes (Appendix 1). To determine sample allocation to strata, the six classes were merged into four classes providing the strata for implementing a stratified random sampling design (Appendix 2). The spatial assessment unit is a Landsat pixel (30 m x 30 m). A binary reference scheme was considered inappropriate for identifying possible reasons for omission and commission related errors and for allocating samples to the different landcover classes (Table 1, p.16). In proportional sample allocation, the sample size per map class is proportional to the relative area of the map classes. Imprecise estimates of user's accuracy in proportional sample allocation are only the case for strata consisting of rare classes (Olofsson et al., 2014). Due to the reduction of classes after the classification, the extents of strata size are considered to be balanced (Appendix 3).

The stratified random sampling satisfies basic accuracy assessment objectives and most of the design criteria, since data from the Landsat open archive in combination with high spatial resolution imagery available through Google Earth are used for validating. It is considered a low-cost and useful source of reference data (Olofsson et al., 2014). The validation labelling was performed similarly to the training data labelling, primarily by using high-resolution imagery in Google Earth. In addition, the same two mean composites for training data collection were used to distinguish winter and spring crops from other arable areas by displaying them in false color.

Since it is not always possible to comply with the probability sampling protocol (Stehman, 2001) all deviations were documented and quantified (Olofsson et al., 2014). In total, 61 reference samples could not be acquired due to mixed-pixels (Choodarathnakara et al., 2012)

or lacking high-resolution imagery in Google Earth (Appendix 3). Of the remaining 839 validation points, 161 were other (forested, urban/ open soil, water), 155 were other arable land, 165 were winter and spring crops and 358 were grassland. To estimate area-adjusted map accuracies and class area proportion, a proportional stratified random sample of the remaining 839 Landsat pixels was used (Olofsson et al., 2014).

To ensure that the reference classification is of higher quality than the map classification, either the reference source must be of higher quality or the process to create the reference classification must be more accurate (Oloffson et al., 2014). To increase the accuracy of the validation process, a confidence rating that represents the perception of uncertainty in the reference classification was included in the reference labelling protocol. Pixels with a low confidence rating were cross checked twice, as small errors in the reference data set can lead to large biases of the estimators of accuracy and class area (Foody, 2010, 2013). The results of the area-adjusted accuracies (overall and class-wise) include 95% Confidence Intervals, the error matrix and adjusted map areas.

Comparison of winter & spring crops with irrigated-summer crops in 2015 and region-specific characteristics at the province-level

According to the definition of Rufin et al (2019), winter and spring crops, as well as summer crops can be subject to double cropping, in which the cultivated plants undergo two growth cycles within one year. In order to be able to decide whether the mapped winter and spring cropping are exclusively cultivated during winter and spring and not cultivated again in summer (double cropping), the result should be compared with the extent of irrigated summer crops in 2015 (Rufin et al., in prep.). The maps were compared, also because the selected time window may include summer crops, as their growth cycles overlap with winter and spring crops (Figure 2, p. 10). Due to the three-month time window, this can only be recorded by a comparative study, as the growth cycles of the summer crops cannot be captured accurately in the period April to June (Figure 2, p. 10). However, these figures do not reflect the total arable land of the GAP, since the class other arable land of the class catalogue (ID 6, Table 1) is not included.

For this purpose, the binary classification (0=other, 1=Winter and Spring crops) was multiplied by 10 and then the binary classification of summer crops (0= other, 1=summer crops) was subtracted. The result are areas of double cropping (values = 9), summer cropping (values = -1) and spring and winter crops (=values = 10). Since the study area provided by Philippe Rufin covers 78,180 km^2 (Appendix 2) and includes areas outside the nine provinces, e.g. parts on Syrian territory, as well as small offsets especially in the border regions, the classification

results were clipped to the parts of the nine provinces that are intersecting with the study area, which adds up to 74,892 km^2 (Appendix 4). Consequently, only Mardin and Şanlıurfa are entirely located in the GAP region. The remaining provinces are only partly within the study area and are not representative of the whole province, but parts of the provinces within the GAP. The clipped and overlaid map was downloaded, quantified and visualized to identify region-specific characteristics at the province-level within the GAP.

4. Results

Data availability

To achieve the first objective of this study, the identification of the best quarterly time window between beginning of March and end of July 2015, the CSO counts were calculated for all five time windows. The GAP region lies within 12 of the WRS-2 (Landsat Worldwide Reference System) tiles (Figure 3).
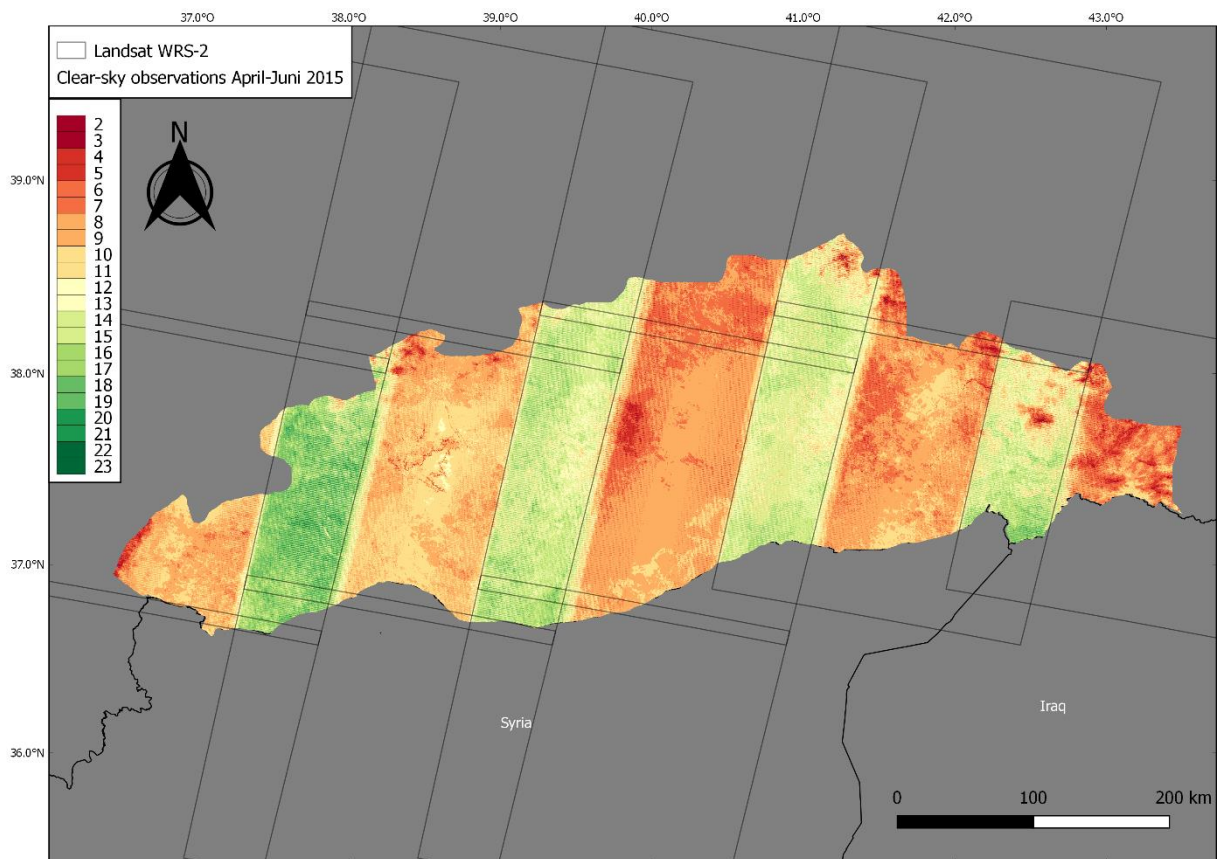
Figure 3. Study area and clear-sky observation count for the period April to June 2015. Overlay represents the 12 Landsat WRS-2 tiles covering the GAP.

After applying the mask functions on all available Landsat 7 and -8 images intersecting with the study area, the image count and mean cloud cover (Table 2, p. 20), as well as the CSO was calculated for five different time windows in 2015 (Table 3, p. 20). The information on cloud

cover contained in the metadata shows a decreasing degree of mean cloud cover from over 27% in the period March to May to under 11% for the May to July period. Contrary to this, the image count which returns the number of elements (scenes) in the collection, increases and since the search is made for the earliest possible period in order to map winter and spring plants as accurately as possible, it is necessary to weigh data availability against accuracy.

Table 2. Statistics on the investigated time-windows.

	March – May	Mid-March– Mid-June	April – June	Mid-April – Mid-July	May – July
Date range	2015-03-03 2015-05-27	2015-03-15 2015-06-12	2015-04-01 2015-06-28	2015-04-15 2015-07-14	2015-05-01 2015-07-30
Image count	118	129	140	146	150
Mean Cloud Cover	27.83%	25.74%	21.31%	15.92%	10.22%

The aim to find at least three CSOs per pixel was not reached by any of the investigated time windows (Table 3). The first two (March to May and mid-March to mid-June) still contain too many unusable pixels (e.g. 0.04% equals 3,207 hectares of no data), even if they both cover more than 98% of the study area with more than three images per pixel (Table 3).

Table 3. Landsat clear observation statistics for the GAP region, 2015.

Time window	Mean CSO count	Maximum CSO count	Percentage No Data	Percentage of Three or More CSOs	Percentage of Five or More CSOs	Percentage of Ten or More CSOs
March-May	8.50	20	0.55%	98.30%	93.01%	34.33%
Mid-March-mid-June	9.41	21	0.04%	99.74%	97.33%	41.71%
April-June	10.97	23	<0.01%	99.95%	99.13%	55.45%
Mid-April-Mid-July	12.53	24	<0.01%	>99.99%	99.91%	78.12%
May-July	13.98	24	<0.01%	>99.99%	99.99%	92.38%

The percentage of data gaps reaches a satisfactory level of 4,673 pixels, which corresponds to about 421 hectares (Appendix 1), for the period April to June, and at the same time fulfils the condition to lie as early as possible in the growth phase of winter and spring plants (Figure 2, p. 10). The mean CSO count is just below 11 images and has a maximum of 23 images. 99.95% of the GAP is covered by three or more CSOs while 99.13% of the study area has five or more valid pixels in this period. The percentage of ten or more valid pixels is 55.45% (Table 3). In total, 140 Landsat scenes were available for the identified three-month time window. The acquisition dates are between 1st April and 28th June and the mean cloud coverage during this period is 21.31% (Table 2). The spatial visualization of CSOs revealed areas of low data coverage and areas with high data availability (Figure 3, p. 19). Those with higher coverage are mainly in the across-track overlap areas, while areas without a single acquisition are mostly located in the mountain regions of the Southeastern Taurus (Güneydogu Toroslar) to the east

of the study area and around the Karaca Dağ shield volcano in the provinces of Şanlıurfa and Diyarbakır. This quarterly time window is chosen for the monitoring of winter and spring crops in the GAP in 2015. It has enough data and covers the growth phase of winter and spring crops (Figure 2, p. 10, blue shading).

Estimating map accuracy, area and confidence intervals

To meet the second objective, the mapping and validation of winter and spring crops in 2015, map accuracy, area and 95% confidence intervals were assessed. Area-adjusted accuracies were calculated including overall and class-wise accuracies for the four strata of the reference classification. The first classification, which was based on 333 training points, reached an overall accuracy of 79.34% (± 2.62%), a producer's accuracy of 90.83% (± 3.71%) and a user's accuracy of 82.82% (± 4.92%), but the process of the reference classification was not as accurate as the final accuracy assessment, as it included low-certainty reference samples (Appendix 5). These could have led to high bias and therefore possibly compromised the representativeness of the results, as small errors in the accuracy assessment can lead to large biases of the estimators of accuracy and class area (Foody, 2010, 2013). Furthermore, the amount of commission related errors of 17.18% was not satisfactorily and therefore another 220 training samples were collected, to reduce errors between faulty classes.

Table 4. Accuracy statistics (area-adjusted calculations).

	Producer's Accuracy	User's Accuracy	Omission Error	Commission Error	Overall accuracy	Producer's Accuracy 95% CI	User's Accuracy 95% CI	Overall Accuracy 95% CI
other arable land	68.18%	55.48%	31.82%	44.52%		7.39%	7.85%	
Winter & spring crops	89.23%	97.58%	10.77%	2.42%		4.13%	2.35%	
Other	87.76%	83.85%	12.24%	16.15%		4.63%	5.70%	
Grassland	84.39%	88.83%	15.61%	11.17%	83.71%	2.88%	3.27%	2.31%

Area-adjusted accuracies for the final classification shows both, strengths and weaknesses of the approach (Table 4). A relatively low overall accuracy of 83.71 (± 2.31%) is partly caused by misclassifications between classes other than winter and spring crops, mainly due to the class other arable land, which has the lowest accuracy. The winter and spring crops class, however, shows accuracies which appear sufficient for the limited scope of this thesis. Class uncertainties are mainly related to the omission of winter and spring crops, which resulted in a producer's accuracy of 89.23% (± 4.13%). Producer's accuracy is lowest for the class other arable land (68.18% ± 7.39%) and class accuracies range between 84.39% (±2.88%) for grassland and 87.76% (±4.68%) for other (includes forested areas, water and open soil/ urban

areas). Users accuracy of 97.58% (± 2.35%) for the winter and spring crops class was highest, while user's accuracies for the other classes ranged from 55.48% (±7.85%) for other arable land, over 83.85% (±5.7%) for the other class to 88.83% (± 3.27%) for the grassland class.

Table 5. *Standard error matrix.*

Classification	Reference				
	Other arable land	Winter & spring crops	Other	Grassland	SUM
Other arable land	86	1	18	50	155
Winter & spring crops	0	161	0	4	165
Other	17	2	135	7	161
Grassland	22	17	1	318	358
SUM	125	181	154	379	839

Main uncertainty factors in the classification are commission errors of 44.52% and omission errors of 31.82% of the other arable land class (Table 4, p. 21). Reasons for the over- as well as underestimation of other arable land are mainly confusion with grassland and other classes. Possible reasons for the relatively high share of omission related errors in the winter and spring crops class (10.77%) are visible in the standard error matrix (Table 5). While the proportion of commission errors is mainly due to the grassland class (4 samples), the omission errors are somewhat more complex. Areas erroneously not counted as winter and spring crops have been classified as grassland (17 samples), other (2 samples) and other arable land (1 sample). In general, however, the underestimation of the winter and spring crops class is most evident due to the confusion with grassland.

Table 6. *Expansion of the four reference strata.*

	Map area (ha)	Adj area (ha)	±CI [ha]	Adj area (%)	±CI [%]	Lower CI	Upper CI
Other arable land	1,396,667	1,136,600	154,679	14.5%	1.98%	981,921	1,291,279
Winter & spring crops	1,588,832	1,737,355	88,639	22.2%	1.13%	1,648,716	1,825,994
Other	1,466,642	1,401,387	111,030	17.9%	1.42%	1,290,357	1,512,417
Grassland	3,365,408	3,542,206	162,099	45.3%	2.07%	3,380,108	3,704,305

Cropland area-adjusted calculations revealed a total expanse of winter and spring crops of 1,737,355 hectares (± 88,639 ha) of land in 2015, which is equal to 22.2% (± 1.13%) of the area of the GAP (Table 6). As for the whole of Turkey (Rufin et al., 2019), winter and spring crops are the dominant cultivated plant in the GAP region. The largest class, however, is that of grassland, which covers 45.3% (± 2.07%) of the study region, while the rarest class, other arable land, covers only 14.5% (± 1.98%). The other class, consisting of water, forested areas, urban/ open soil, covers 17.9% (± 1.42%) of the GAP area.

Comparison of winter & spring crops with irrigated-summer crops in 2015 and region-specific characteristics at the province-level
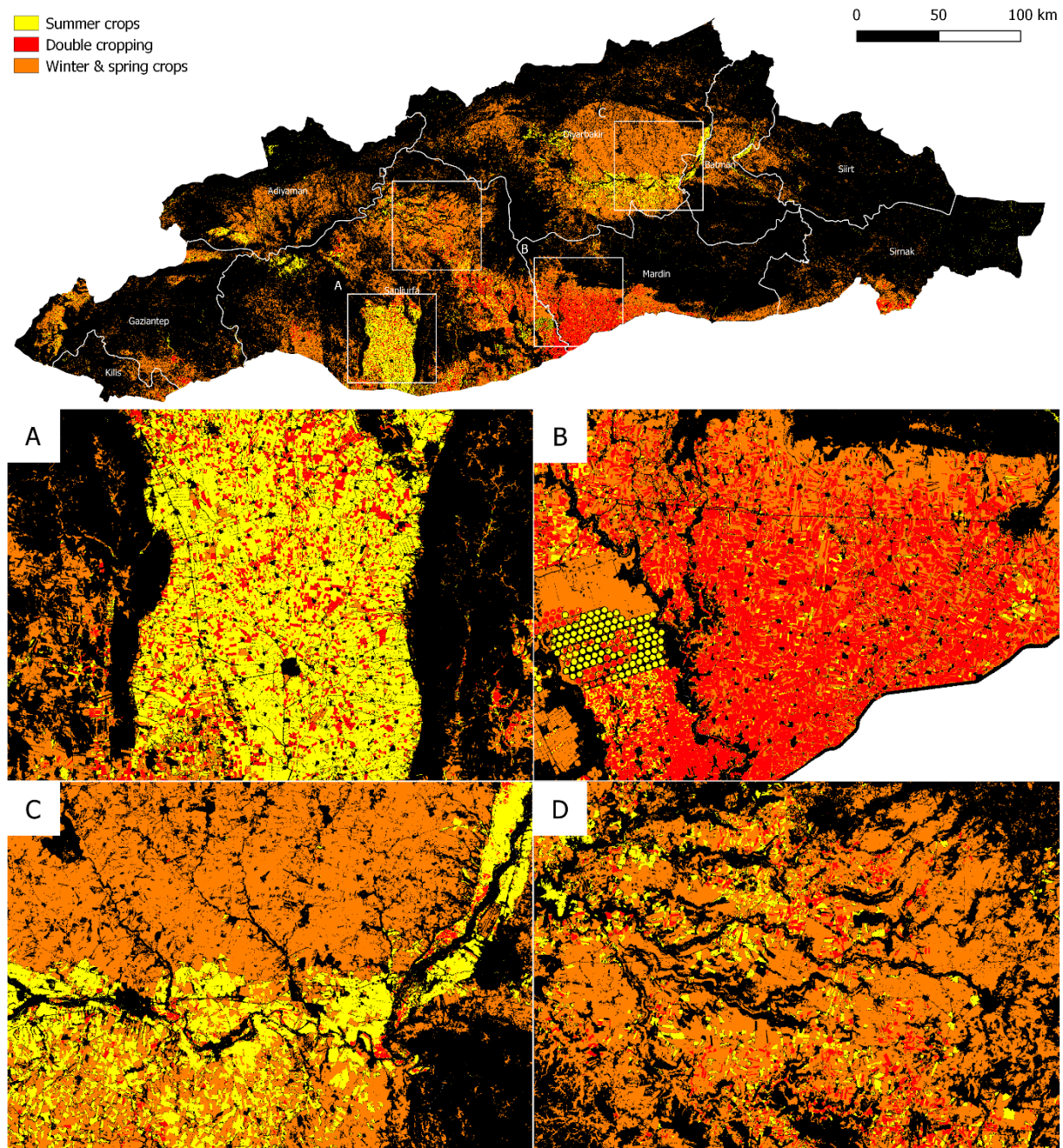
***Figure 4**. Results of the comparison of winter and spring crops with summer crops (Rufin et al., in prep.) and their overlap areas (double cropping) in 2015 in the GAP (upper section) and for selected areas (lower section).*

The resulting map includes areas covered by winter and spring crops, which were not cultivated again in the same year, as well as summer cropped areas (Figure 4). Additionally, areas experiencing double cropping in 2015 can be determined. However, the following results are a combination of two different classifications, and therefore accuracies may decrease. After the classifications were overlaid and cut to the parts of the nine provinces lying within the study

region, winter and spring crops still covered about 1,354,999 hectares of land, summer crops 313,928 hectares and 217,330 hectares of land undergo double cropping in 2015 (Appendix 4). In contrast to irrigated summer crops, the distribution of winter and spring crops is not limited on specific areas (Figure 4, p. 23). Spatially explicit patterns reveal differences in cropping extent and practice across and within regions. Most evident expansion was mainly located in parts south of the Taurus mountains in Diyarbakır (Figure 4 C, p. 23) and in northern Şanlıurfa (Figure 4 D, p. 23). Summer crops, on the other hand, expand over large parts of Şanlıurfa's Harran plain (Figure 4 A, p. 23) and along the Tigris river valleys in Southeastern Diyarbakır (Figure 4 C, p. 23). Before the irrigated summer crops mask was applied and double cropped areas where subtracted, they were mainly located in the central and southern provinces of Şanlıurfa, Mardin, and Diyarbakır (Rufin et al., in prep.). Thus, the detected double cropped areas are spatially represented in southwestern Mardin and the east of Şanlıurfa (Figure 4 B, p. 23).
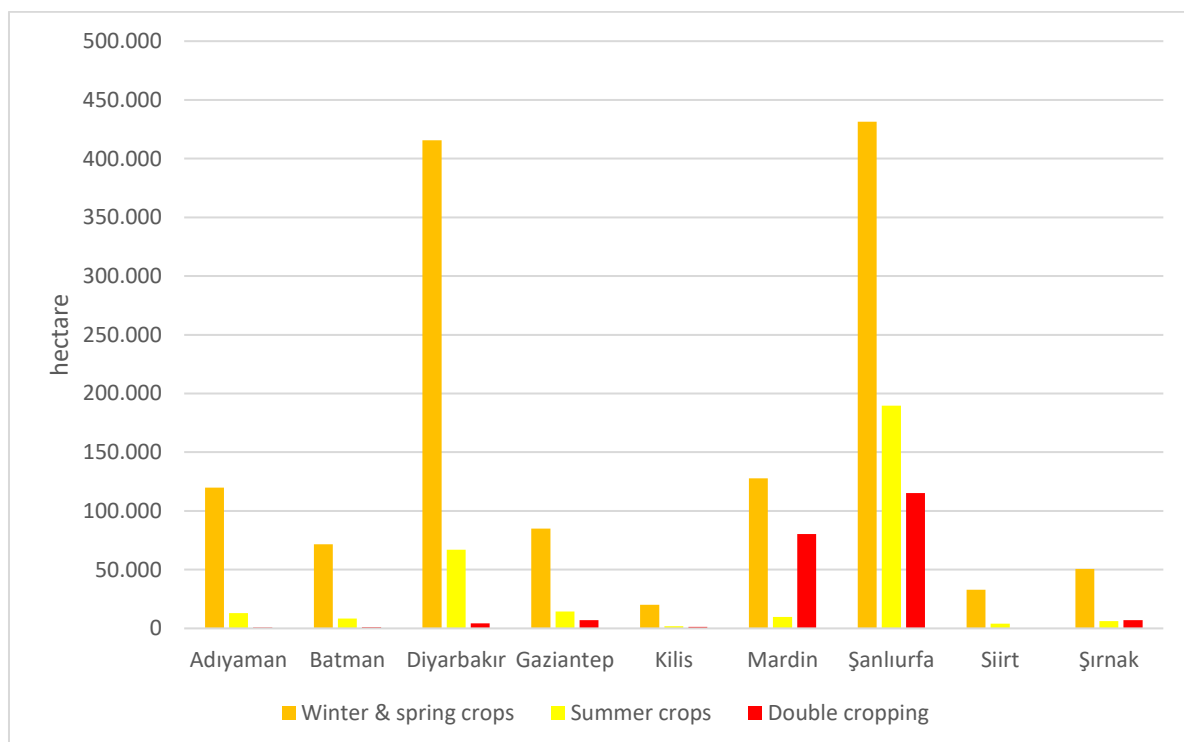
Figure 5. Total cropland expanse of the different cropping practices by province in 2015.

The total cropland expanse of the three different cropping practices by province in 2015 are shown in Figure 5. These figures do not reflect the total arable land of the GAP, but the land cultivated either in summer crops or in winter and spring and their overlapping areas identified by this study and the comparative study (Rufin et al., in prep.). Since other cultivated areas, like pistachio and olive trees were not included in the class catalogs in both studies, this extent is not the absolute cultivable area in the GAP. However, the total area covered by all three classes

was highest in Şanlıurfa (736,365 ha), Diyarbakır (487,059 ha) and Mardin (217,592 ha). The absolute largest expansion of winter and spring crops are in Diyarbakır (415,739 ha) and Şanlıurfa (431,525 ha). Least spread they are in Şırnak (50,569 ha), Siirt (33,026 ha) and Kilis (20,078 ha). Double cropping, on the contrary, takes place mainly in Şanlıurfa (115,177 ha) and Mardin (80,232 ha, Appendix 4).
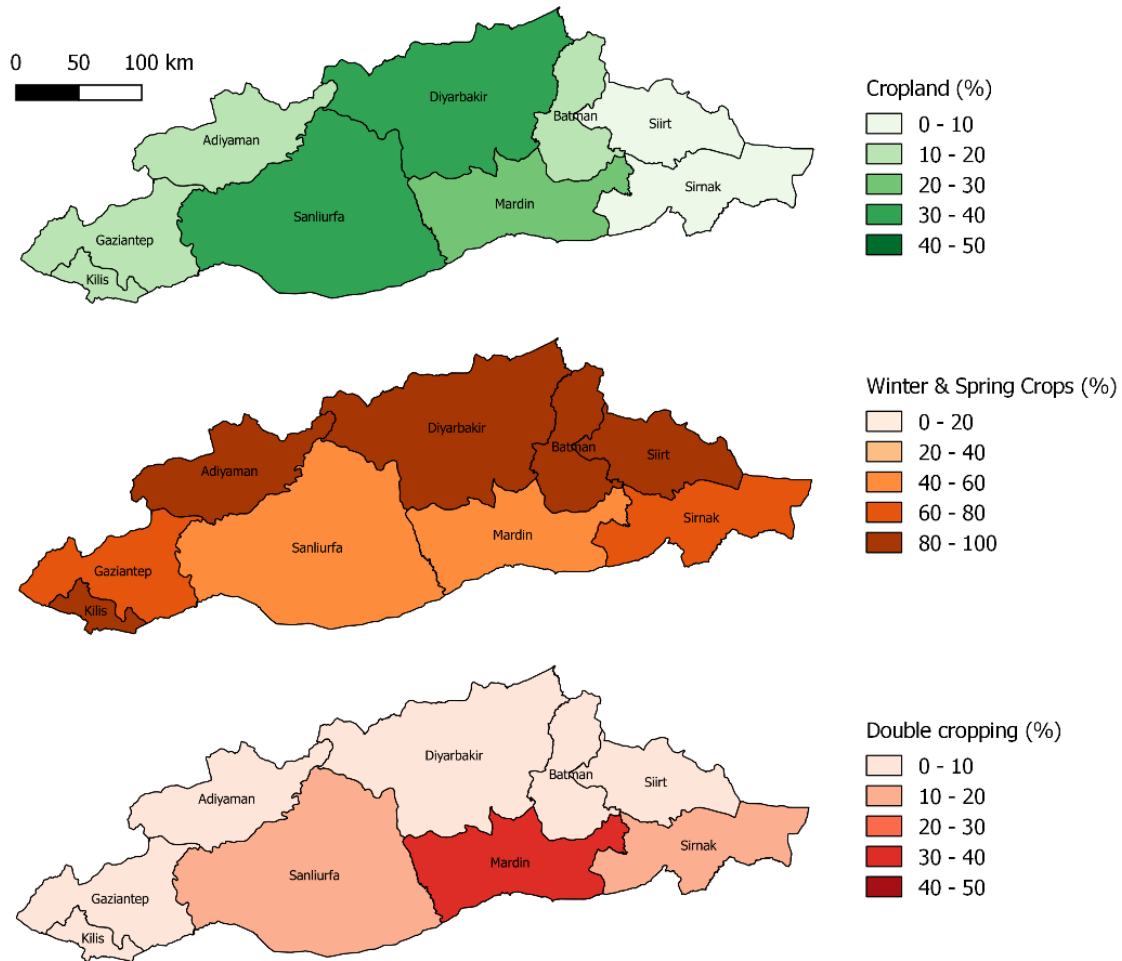
Figure 6*. Province-level (NUTS-03) share of cropland expansion (winter & spring crops, summer crops and double cropping) on total province area within the GAP (top) and share of winter & spring crops (middle) as well as double cropping (bottom) in percent of all cropland in 2015.*

Province-level (NUTS-3) shares of cropland, winter and spring crops and double cropping practices of the parts of the provinces within the GAP are shown in Figure 6. The share of all detected cropland of the total area is highest in Şanlıurfa and Diyarbakır (30-40%), still accounts for more than 20% in Mardin, but is less than 20% in all other regions, and even less than 10% in Siirt and Şırnak (Figure 6, top).

The highest proportion of winter and spring crops on agricultural land (>80%) is found in the provinces of Kilis, Adıyaman, Diyarbakır, Batman and Siirt (Figure 6, middle). Just over 79%

of the cropland of Gaziantep and Şırnak is cultivated exclusively in spring and winter (Appendix 4), while the proportion is between 40 and 60% in Şanlıurfa and Mardin.

While Rufin et al. (in prep.) noted a high density of summer crops in the Şanlıurfa province, especially in the Harran plain, the intensive cultivation of agricultural land in Mardin is largely (36.87%, Appendix 4) attributed to double cropping practices. Double cropping is also present in Şanlıurfa and Şırnak (10-20%, Figure 6, p. 25, bottom), whereas moderate intensive double cropping is practiced in the remaining provinces. The province-level statistics reported here, are well in line with the study by Rufin et al. (2019). Deviations however, may be due to slightly different class catalogues and due to the area investigated, as the results presented here represent the province parts within the GAP region, not the whole province.

5. Discussion

This study presents a satellite-based characterization of the extent of winter and spring crops in the GAP region in 2015. The extent at 30 m spatial resolution was derived by using pixel-based compositing and by training a non-parametric random forest classifier to predict spectral-temporal metrics. The approach offers the opportunity to assess the current extent of winter and spring crops in the GAP region, assuming that Landsat-based spectral-temporal metrics provide valuable information on the phenology of land, similar to recent studies (Griffiths et al., 2018; Rufin et al., in prep.). The initial intention to create change maps for winter and spring crops, following the example of Rufin et al. (in prep.), were not within the scope of this thesis. However, the here presented approach could be transferred to create annual change maps for winter and spring crops, assuming sufficient data availability.

Data availability

As data availability was considered the limiting factor, the quarterly time window from 1st April until 26th June was chosen as a trade-off between data availability and temporal detail. In total, 140 scenes across 12 WRS-2 tiles were used for compositing and for computing spectral-temporal variability metrics. Although this three-month time window had a mean cloud cover of 21.31% (Table 2, p. 20), on average more than ten images per pixel were available and 99.95% of the study area had at least three valid images per pixel after masking clouds, cloud-shadows and snow (Table 3, p. 20). Besides higher cloud cover in winter and the early spring months, data-scarce areas are also due to snow-covered mountain regions of the Southeastern Taurus (Güneydogu Toroslar) and around Karaca Dağ shield volcano in the provinces of

Şanlıurfa and Diyarbakır. In the eastern Anatolian mountains, the high winter precipitation is largely stored as ice and snow (Glaser and Kremb, 2013).

Data gaps could be overcome by synthetic Gap Filling techniques (Schwieder et al. 2016; Rufin et al., 2019). These techniques lead to improved mapping accuracies when compared to non-gap-filled features (Griffiths, Nendel & Hostert, 2019). However, in this study no gap-filling techniques were used, because according to Senf et al. (2015), algorithms can be used to compensate for data gaps, but if Landsat data availability is sufficient to cover all phenological important dates, the dependency on Landsat alone is considered satisfactory.

Another negative factor influencing the data availability is the loss of the Scan Line Corrector (SLC) onboard Landsat 7 in May 2003 (Markham et al., 2004). Among other reasons, this is mentioned as a factor that increases the likelihood of data gaps in Landsat, producing temporal and spatial discontinuities in Landsat data (Wulder et al., 2008). Since misclassifications can occur in data-scarce areas (Schwieder et al. 2016), the influence of the failure of SLC was visually noticeable (Appendix 6). The original intention to have at least three CSOs per pixel seems to be too low considering the unrecorded winter and spring crops in areas with less than five CSOs (Appendix 6). But despite the SLC failure, the USGS keeps delivering data from Landsat 7, in a form that meets the observation requirements (Cohen & Goward, 2004), and therefore this has been neglected in this study.

Apart from the possible influence of the SLC failure (Appendix 6), no statistical correlations between data availability and misclassifications for winter and spring crops could be detected, within the scope of this study. Nevertheless, this should be investigated more closely to better understand variation of accuracy determined by observation density, for instance, by using the count of CSOs as strata for validation or by linear regression analyses between the annual number of clear observations and reached accuracies (Rufin et al., in prep.).

The across-track overlap areas had a positive influence on the data availability (Figure 3). Since the Landsat data are acquired on the WRS-2 path/row system, with swath overlap varying from 7% at the Equator to a maximum of approximately 85% at extreme latitudes (NASA, 2019; USGS 2019d), these overlapping areas are responsible for the high CSO counts (Table 3). Although WRS-row overlap was neglected, the higher data availability in the across track overlap and the lower data availability in the mountainous area of Şırnak and Siirt are well along with a current study mapping cropping practices on a national-scale (Rufin et al., 2019). To overcome restrictions in data availability, Griffiths, Nendel & Hostert (2019) recommend the combination of Sentinel with Landsat data to assess agricultural and other land-use over large areas. Senf et al. (2015) include coarse spatial resolution data from the MODerate-

resolution Imaging Spectroradiometer to close data gaps, whereas Pflugmacher et al. (2019) suggest the combination of remote sensing methods with other land cover products, such as the European LUCAS survey database. Another possible solution for overcoming data availability constraints and simultaneously capturing exclusively winter and spring crops would be to consider appropriate time-windows separately for each province.

Methods and classification accuracies

An overall accuracy of 83.71% (± 2.31%) and producer's accuracy of 89.23% (± 4.13%) and user's accuracy of 97.58% (± 2.35%) for winter and spring crops, indicate the robustness of the approach and reveal the possible transferability to earlier periods for creating annual change maps for winter and spring crops, assuming sufficient data availability. However, a relatively high share of omission error of 10.77% largely corresponds to the grassland class, at the expense of the winter and spring cropping class.

The most common error influencing the accuracy of the winter and spring crops class was between winter and spring crops and grassland (Table 5, p. 22). The reasons for this may lie in the heterogeneity within the classes (crop type, grass species, phenology, planting date and density) and in spectral-temporal similarities between classes. One possible reason for the confusion of winter and spring crops and grassland is, that both classes represent herbaceous vegetation areas, which exhibit precipitation-driven phenology and underly management interventions (Rufin et al., 2019). Rufin et al. (in prep.) point out, the variation of accuracy may also be depending on the temporal distribution of the observations relative to the phenological cycles of the crops. These are not only region-specific (Figure 2, p. 10), but also dependent on precipitation and temperature patterns (Section 2).

Furthermore, varying sensor constellations and cloud-contaminated areas are found to potentially compromise the consistency of spectral-temporal metrics (Rufin et al., in prep.). Even though inaccuracies between similar classes are not uncommon (Schwieder et al., 2016), more frequent satellite observations can help to increase accuracy of artificial land and cropland (Pflugmacher et al., 2019). However, the grassland class is most probably overestimated, as it included permanent pastures, which accounted for 14.6 million hectares in Turkey in 2015 (TSI, 2015) as well as sparsely covered areas, which could also be considered open soil (Table 1, p.16). The underestimation of the expansion of winter and spring crops in 2015, on the other hand, can also be attributed to misclassifications and unrecorded areas due to the influence of the SLC failure (Appendix 6). In summary, it can be stated that the confusion between the grassland and winter crops classes leads to an underestimation of winter and spring crops class.

Since there was a lack of validation data (ground truth), the area-adjusted accuracy assessment estimation had to be used (Olofsson et al., 2014). This process is very time-consuming as sufficient samples need to be validated to minimize the effects of errors. Nevertheless, actual accuracies may vary as they are only estimated, a problem that could be solved by additional interpreters cross-checking the validation samples. However, the accuracy of the winter and spring crops class achieved adequate results in the final classification, so that the iterative process of random forest classification was ended after the results presented here were achieved (Breiman, 2001). Higher accuracies could have been achieved, by collecting more training points or by using polygon-based samples instead of pixels-based. However, these samples had to be accurate, whereas a higher level of expertise about the study area was necessary. But since the pixel-based approach makes it possible to capture areas that are not subject to a defined minimum mapping unit, this approach was chosen. However, in the course of the validatin it became clear that single isolated pixels were often wrongly classified. In order to increase the accuracy, it would be necessary to consider whether these should be excluded. Nevertheless, errors can also occur during the training data search, which also can be reduced by additional trained interpreters. The mixed-pixel effect prevented the validation of 48 samples (Appendix 3). Mixed pixels affect the use of remotely sensed data in classification, this issue can be addressed by adopting soft classification methods based on Fuzzy Logic and Artificial Neural Networks (Choodarathnakara et al., 2012).

Comparison of winter & spring crops with irrigated-summer crops in 2015 and region-specific characteristics at the province-level

Although irrigated summer crops in the GAP reached 577,887 ha (± 47,932) in 2018, which corresponds to 617% increase since 1990 (Rufin et al., in prep.), winter and spring crops are the dominant cropping practice covering 1,737,355 hectares (± 88,639 ha) of land of the GAP region in 2015. It is possible, though, that the chosen time window was unfavorable as it may include summer crops, which intersect with the growth cycles of winter and spring crops (Figure 2, p.10). For instance, most of its cotton is planted between mid-March and mid-May, and harvested from mid-August through November (USDA, 2019) and may therefore have been mistakenly recorded as winter and spring crops.

Regarding the absolute area, Rufin et al. (in prep.) clarify that the expansion of summer cropping concentrated widely in the central and southern provinces (Şanlıurfa, Mardin, and Diyarbakır). This study reveals that the intensive cultivation of agricultural land in Mardin is largely attributed to double cropping (Figure 4 B, p. 23). The high share of double cropping in

Mardin is likely related to the cultivation of winter cereals in rotation with corn (Rufin et al., in prep.) since cotton does not allow for double cropping and the cotton fields therefore often lie fallow in winter and spring (Özdoğan et al., 2006).

Although this study could not reveal any clear implications on water usage, preferences for rain-fed agriculture are apparent, as they were before the initiation of the GAP (Metin Sezen and Yasar, 2006). But even if winter and spring crops, such as cereals and pulses, have a low water requirement and are mainly rain-fed, they are also irrigated. Since they are usually harvested mid to late May, these fields cannot support winter and spring crops as well as summer crops in the same year. The contradictory growth plan with winter plants does not permit double cropping of cotton and so the cotton fields often lie fallow in winter and spring (Özdoğan et al., 2006). Other reasons for rainfed instead of irrigated cropping are mainly economic, technical and managerial constraints, which vary according to the irrigation and maintenance institutions (Harris, 2009; Kibaroğlu et al., 2011). Aggravating is the low overall efficiency of irrigation practices, which is primarily driven by water losses due to evaporation, interception and conveyance (Jägermeyr et al., 2015). Furthermore, as Rufin et al. (in prep.) stated, an average half of the irrigation infrastructure remains idle at an annual basis and concluded, that investments are not used to their potential.

In many irrigated regions, mostly those with already high shares of irrigated agriculture, freshwater restrictions may even require the conversion of arable land from irrigated to rain-managed irrigation in the future. Irrigation is not enough to compensate for the effects of climate change on current agricultural land. The main drivers for this effect are water limitations and population growth (Elliott et al., 2014). To mitigate the risks of water scarcity and soil salinization in arid and semi-arid regions, Singh (2016) proposes strategies such as changes in cropping patterns, reduced canal water use, or increased groundwater use and canal lining.

It reveals the need for more efficient management of arable land with less water and land use. In addition, the potential to reduce the yield gap in rainfed systems is much greater, mainly for economic reasons. Against the background of climate change, which could even reduce current yield differentials, there is a considerable need for action (Lobell et al., 2009). Ultimately, food production could be doubled without further reducing the environmental impact of agriculture. This, however, requires strategies that go hand in hand. These include curbing agricultural expansion, closing yield gaps, increasing crop efficiency, shifting eating habits and reducing waste. However, successful implementation of this policy requires reforms in world trade to eliminate price-distorting subsidies and tariffs (Foley et al., 2011).

However, a sustainable expansion and intensification of irrigation could help to achieve food security and environmental goals without ultimately exhausting environmental flows. But to achieve this, adequate and informed investments in irrigation infrastructure and the implementation of monitoring systems should reduce dependence on the use of non-renewable freshwater resources (Rosa et al., 2018). An alternative to further cropland expansion or conversion to monoculture croplands are rural development polices. These should focus on improving socio-economic conditions of rural areas to decline the pressure on freshwater resources through water reuse, desalination, the construction of dams and channels and eventually increasing the efficiency of rainfed cropland (Malek et al., 2018).

6. Conclusion

Remote sensing can help to meet the growing need for spatial information on agricultural land (Bégué et al., 2018) by improving the understanding of the spatial-temporal variability of agricultural systems across administrative boundaries (Deines et al., 2017). Landsat-based data analyses have shown that they offer the capability to map the extent of cropland over large areas at 30 m spatial resolution (Rufin et al., 2019). This study used exclusively freely available satellite time series (Landsat Collection 1 Surface Reflectance), accessed and pre-processed through the cloud-based Google Earth Engine (Gorelick et al., 2017), to quantify the expansion of winter and spring crops in Southeastern Anatolia in 2015. The combination of a Random Forest classification algorithm with quarterly Landsat-based composites and spectral-temporal metrics achieved good classification results. Within the scope of this study, benefits of the freely available Landsat data for mapping cropping practices over large areas using time series in combination with Google Earth Engine became clear. It is now possible for non-specialists with limited access to resources and short time frames to create large-scale maps. However, debugging was a challenging task, especially for novices.

As Rufin et al. (2019) points out, the combination of quarterly composites and spectral-temporal metrics offers great opportunities to map cropping practices, but not for data-scarce quarters. They recommend including feature sets such as geographic location (latitude, longitude) and topography (elevation, slope) as auxiliary variables to increase overall accuracy. Since more frequent satellite observations are found to increase accuracy of artificial land and cropland (Pflugmacher et al., 2019), higher classification accuracies could have been achieved by the integration of additional satellite data like Sentinel (Griffiths, Nendel & Hostert, 2019) or MODIS (Senf et al., 2015). Another approach to increase accuracies are gap-filling techniques

(Rufin et al., 2019) or the combination of remote sensing methods with other land cover products, such as the European LUCAS survey database (Pflugmacher et al., 2019).

However, the period April to June covered all phenologically important data and had sufficient data availability. Therefore, this study was based solely on the use of spectral-temporal metrics and quarterly compositing for mapping winter and spring crops in the GAP. An overall accuracy of 83.71 ($\pm$ 2.31%), producer's accuracy of 89.23% ($\pm$ 4.13%) and user's accuracy of 97.58% ($\pm$ 2.35%) for the winter and spring crops class indicate the strength of this approach. However, further research on the robustness of spectral-temporal metrics under changing observation densities is needed, as influences of the SLC failure on unrecorded winter and spring crops were discernible (Appendix 6). Although residual uncertainties remain, the here presented results indicate, that 217,330 hectares were cropped twice in 2015, while winter and spring crops covered about 1,354,999 hectares of land in 2015.

As Ray and Foley (2013) point out, an increasing frequency of global cultivation can boost crop yields through additional cultivation cycles. Singh (2016) suggests strategies such as changes in cropping patterns, reduced canal water use, increased groundwater use and canal lining. However, the cotton fields in the GAP do not support double cropping and therefore often lie fallow in winter and spring (Özdoğan et al., 2006), but at the same time account for half of the cotton grown in Turkey (USDA, 2019).

As agricultural expansion is no longer feasible in most parts of the world (Porkka et al., 2016) and the enhanced input of water, fertilizer and pesticides (Erb et al., 2013; Foley et al., 2011) raise the risks of water scarcity and soil salinization (Mekonnen and Hoekstra, 2016) a more sustainable management of water ought to reduce the reliance on the use of non-renewable freshwater resources (Rosa et al., 2018).

Some studies conclude that irrigated arable land should be converted into rain-fed management in the future, as irrigation is not suitable to compensate for varying climatic influences due to fresh water shortages and population growth (Elliott et al., 2014). Foley et al. (2011) recommend, that strategies like halting agricultural expansion, closing yield gaps, increasing cropping efficiency shifting diets and reducing waste should go hand in hand. This could ultimately double food production without further harming environmental impacts of agriculture. Albeit for the successful implementation of these policies reforms in global trade to eliminate price-distorting subsidies and tariffs are required.

7. Acknowledgement

References

Altinbilek, D., & Tortajada, C. (2012). The Atatürk Dam in the context of the Southeastern Anatolia (GAP) project. In *Impacts of large dams: A global assessment* (pp. 171-199). Springer, Berlin, Heidelberg.

Ambika, A. K., Wardlow, B., & Mishra, V. (2016). Remotely sensed high resolution irrigated area mapping in India for 2000 to 2015. *Scientific data*, *3*, 160118.

Bégué, A., Arvor, D., Bellon, B., Betbeder, J., De Abelleyra, D., PD Ferraz, R., Lebourgeois, V., Lelong, C., Simões, M. & R Verón, S. (2018). Remote sensing and cropping practices: A review. *Remote Sensing*, *10*(1), 99.

Bilgen, A. (2018a). The Southeastern Anatolia Project (GAP) in Turkey: An Alternative Perspective on the Major Rationales of GAP. *Journal of Balkan and Near Eastern Studies*, 1-21.

Bilgen, A. (2018b). The Southeastern Anatolia Project (GAP) revisited: The evolution of GAP over forty years. *New Perspectives on Turkey*, *58*, 125-154.

Breiman, L. (2001). Random forests. *Machine learning*, *45*(1), 5-32.

Choodarathnakara, A. L., Kumar, T. A., Koliwad, S., & Patil, C. G. (2012). Mixed pixels: a challenge in remote sensing data classification for improving performance. *International Journal of Advanced Research in Computer Engineering & Technology (IJARCET)*, *1*(9), 261.

Cochran, W. G. (1977). Sampling techniques-3.

Cohen, W. B., & Goward, S. N. (2004). Landsat's role in ecological applications of remote sensing. *Bioscience*, *54*(6), 535-545.

Deines, J.M., Kendall, A.D., & Hyndman, D.W. (2017). Annual Irrigation Dynamics in the U.S. Northern High Plains Derived from Landsat Satellite Data. *Geophysical Research Letters*, *44*, 475 9350–9360.

Dinerstein, E., Olson, D., Joshi, A., Vynne, C., Burgess, N. D., Wikramanayake, E., ... & Hansen, M. (2017). An ecoregion-based approach to protecting half the terrestrial realm. *BioScience*, *67*(6), 534-545. Available online: https://ecoregions2017.appspot.com/ (accessed on 8 September 2019).

Dong, J., Xiao, X., Menarguez, M. A., Zhang, G., Qin, Y., Thau, D., Biradar, C. & Moore III, B. (2016). Mapping paddy rice planting area in northeastern Asia with Landsat 8 images, phenology-based algorithm and Google Earth Engine. *Remote sensing of environment*, *185*, 142-154.

Elliott, J., Deryng, D., Muller, C., Frieler, K., Konzmann, M., Gerten, D., Glotter, M., Florke, M., Wada, Y., Best, N., Eisner, S., Fekete, B.M., Folberth, C., Foster, I., Gosling, S.N., Haddeland, I., Khabarov, N., Ludwig, F., Masaki, Y., Olin, S., Rosenzweig, C., Ruane, A.C., Satoh, Y., Schmid, E., Stacke, T., Tang, Q., & Wisser, D. (2014). Constraints and potentials of future irrigation water availability on agricultural production under climate change. *Proceedings of the National Academy of Sciences of the United States of America*, *111*, 3239–3244. Available online: https://doi.org/10.1073/pnas.1222474110 (accessed on 8 September 2019).

Erb, K. H., Haberl, H., Jepsen, M. R., Kuemmerle, T., Lindner, M., Müller, D., Verburg, P. H. & Reenberg, A. (2013). A conceptual framework for analysing and measuring land-use intensity. *Current opinion in environmental sustainability*, *5*(5), 464-470.

FAO (2009). Irrigation in the Middle East Region. Country Profile: Turkey; AQUASTAT Survey-   2008 No. 34; FAO: Rome, Italy.

Foga, S., Scaramuzza, P. L., Guo, S., Zhu, Z., Dilley Jr, R. D., Beckmann, T., Schmidt, G. L., Dwyer, J. L., Hughes, M. J. & Laue, B. (2017). Cloud detection algorithm comparison and validation for operational Landsat data products. *Remote sensing of environment*, *194*, 379-390.

Foley, J. A., Ramankutty, N., Brauman, K. A., Cassidy, E. S., Gerber, J. S., Johnston, M., Mueller, N. D., O'Connell, C., Ray, D. K., West, P. C., Balzer, C., Bennett, E. M., Carpenter, S. R., Hill, J., Monfreda, C., Polasky, S., Rockström, J., Sheehan, J., Siebert, S., Tilman, D. & Zaks, D. P. M. (2011). Solutions for a cultivated planet. *Nature*, *478*(7369), 337.

Foody, G. M. (2010). Assessing the accuracy of land cover change with imperfect ground reference data. *Remote Sensing of Environment*, *114*(10), 2271-2285.

Foody, G. M. (2013). Ground reference data error and the mis-estimation of the area of land cover change as a function of its abundance. *Remote Sensing Letters*, *4*(8), 783-792.

Fritz, S., See, L., McCallum, I., You, L., Bun, A., Moltchanova, E., ... & Havlik, P. (2015). Mapping global cropland and field size. *Global change biology*, *21*(5), 1980-1992.

GAP (2019a). GAP Regional Development Administration. What's GAP. http://www.gap.gov.tr/en/index.php (accessed on 8 September 2019).

GAP (2019b). GAP Regional Development Administration. History of GAP. http://www.gap.gov.tr/en/history-page-3.html (accessed on 8 September 2019).

GAP (2019c). GAP Regional Development Administration. Latest state in GAP. http://www.gap.gov.tr/en/latest-state-in-gap-page-47.html (accessed on 8 September 2019).

Gerten, D., Heinke, J., Hoff, H., Biemans, H., Fader, M., & Waha, K. (2011). Global water availability and requirements for future food production. *Journal of hydrometeorology*, *12*(5), 885-899.

Glaser, Rüdiger & Kremb, Klaus (2013). Planet Erde. Asien. Das Wasser von Euphrat und Tigris: Die Instrumentalisierung einer natürlichen Ressource. S. 29-42

Google Developers (2019). Earth Engine Data Catalog. USGS Landsat 8 Surface Reflectance Tier 1. https:// developers.google.com/earth-engine/datasets/catalog/LANDSAT_LC08_C01_T1_SR (Accessed on 8 September 2019).

Gorelick, N., Hancher, M., Dixon, M., Ilyushchenko, S., Thau, D., & Moore, R. (2017). Google Earth Engine: Planetary-scale geospatial analysis for everyone. *Remote Sensing of Environment*, *202*, 18-27.

Griffiths, P., Nendel, C., & Hostert, P. (2019). Intra-annual reflectance composites from Sentinel-2 and Landsat for national-scale crop and land cover mapping. Remote sensing of environment, 220, 135-151.

Griffiths, P., Jakimow, B., & Hostert, P. (2018). Reconstructing long term annual deforestation dynamics in Pará and Mato Grosso using the Landsat archive. *Remote sensing of environment*, *216*, 497-513.

Griffiths, P., van der Linden, S., Kuemmerle, T., & Hostert, P. (2013). A Pixel-Based Landsat Compositing Algorithm for Large Area Land Cover Mapping. *IEEE Journal of Selected Topics in Applied Earth Observations and Remote Sensing*, *6*, 2088–2101.

Hansen, M. C., Potapov, P. V., Moore, R., Hancher, M., Turubanova, S. A. A., Tyukavina, A., Thau, D., Stehman, S. V., Goetz, S. J., Loveland, T. R., Kommareddy, A., Egorov, A., Chini, L., Justice, C. O. & Townshend, J. R. G. (2013). High-resolution global maps of 21st-century forest cover change. *science*, *342*(6160), 850-853.

Harris, L. M. (2009). Contested sustainabilities: Assessing narratives of environmental change in southeastern Turkey. *Local Environment*, *14*(8), 699-720.

Hommes, L., Boelens, R., & Maat, H. (2016). Contested hydrosocial territories and disputed water governance: Struggles and competing claims over the Ilisu Dam development in southeastern Turkey. *Geoforum*, *71*, 9-20.

Johansson, E. L., Fader, M., Seaquist, J. W., & Nicholas, K. A. (2016). Green and blue water demand from large-scale land acquisitions in Africa. *Proceedings of the National Academy of Sciences*, *113*(41), 11471-11476.

Ju, J., & Roy, D. P. (2008). The availability of cloud-free Landsat ETM+ data over the conterminous United States and globally. *Remote Sensing of Environment*, *112*(3), 1196-1211.

Kibaroğlu, A., Scheumann, W., & Kramer, A. (Eds.). (2011). *Turkey's water policy: national frameworks and international cooperation*. Springer Science & Business Media.

Kottek, M., J. Grieser, C. Beck, B. Rudolf, and F. Rubel. (2006): World Map of the Köppen-Geiger climate classification updated. *Meteorol. Z.*, 15, 259-263. Available online: http://dx.doi.org/10.1127/0941-2948/2006/0130 (accessed on 8 September 2019).

Kovalskyy, V., & Roy, D. P. (2013). The global availability of Landsat 5 TM and Landsat 7 ETM+ land surface observations and implications for global 30 m Landsat data product generation. *Remote Sensing of Environment*, *130*, 280-293.

Kovalskyy, V., & Roy, D. P. (2015). A one year Landsat 8 conterminous United States study of cirrus and non-cirrus clouds. *Remote Sensing*, *7*(1), 564-578.

Lobell, D. B., Cassman, K. G., & Field, C. B. (2009). Crop yield gaps: their importance, magnitudes, and causes. *Annual review of environment and resources*, *34*, 179-204.

Lopes, M. S., Royo, C., Alvaro, F., Sanchez-Garcia, M., Ozer, E., Ozdemir, F., Karaman, M., Roustaii, M., Jalal-Kamali, M. R. & Pequeno, D. (2018). Optimizing winter wheat resilience to climate change in rain fed crop systems of Turkey and Iran. *Frontiers in plant science*, *9*, 563.

Malek, Ž., Verburg, P. H., Geijzendorffer, I. R., Bondeau, A., & Cramer, W. (2018). Global change effects on land management in the Mediterranean region. *Global Environmental Change*, *50*, 238-254.

Markham, B. L., Goward, S., Arvidson, T., Barsi, J., & Scaramuzza, P. (2006). Landsat-7 long-term acquisition plan radiometry-evolution over time. *Photogrammetric Engineering & Remote Sensing*, *72*(10), 1129-1135.

Markham, B. L., Storey, J. C., Williams, D. L., & Irons, J. R. (2004). Landsat Sensor Performance: History and current status. IEEE Transactions on Geoscience and Remote Sensing, 42, 2691−2694.

Mekonnen, M. M., & Hoekstra, A. Y. (2016). Four billion people facing severe water scarcity. Science advances, 2(2), e1500323.

Metin Sezen, S., & Yazar, A. (2006). Wheat yield response to line-source sprinkler irrigation in the arid Southeast Anatolia region of Turkey. *Agricultural Water Management*, *81*, 59–76.

Müller, H., Rufin, P., Griffiths, P., Siqueira, A. J. B., & Hostert, P. (2015). Mining dense Landsat time series for separating cropland and pasture in a heterogeneous Brazilian savanna landscape. *Remote Sensing of Environment*, *156*, 490-499.

NASA (2019). The Worldwide Reference System. https://landsat.gsfc.nasa.gov/the-worldwide-reference-system/ (accessed on 8 September 2019).

Oliphant, A. J., Thenkabail, P. S., Teluguntla, P., Xiong, J., Gumma, M. K., Congalton, R. G., & Yadav, K. (2019). Mapping cropland extent of Southeast and Northeast Asia using multi-year time-series Landsat 30-m data using a random forest classifier on the Google Earth Engine Cloud. *International Journal of Applied Earth Observation and Geoinformation*, *81*, 110-124.

Olofsson, P., Foody, G. M., Herold, M., Stehman, S. V., Woodcock, C. E., & Wulder, M. A. (2014). Good practices for estimating area and assessing accuracy of land change. *Remote Sensing of Environment*, *148*, 42-57.

Özdoğan, M., Woodcock, C. E., Salvucci, G. D., & Demir, H. (2006). Changes in summer irrigated crop area and water use in Southeastern Turkey from 1993 to 2002: Implications for current and future water resources. *Water resources management*, *20*(3), 467-488.

Pekel, J. F., Cottam, A., Gorelick, N., & Belward, A. S. (2016). High-resolution mapping of global surface water and its long-term changes. *Nature*, *540*(7633), 418.

Pflugmacher, D., Rabe, A., Peters, M., & Hostert, P. (2019). Mapping pan-European land cover using Landsat spectral-temporal metrics and the European LUCAS survey. *Remote sensing of environment*, *221*, 583-595.

Phalke, A. R., & Özdoğan, M. (2018). Large area cropland extent mapping with Landsat data and a generalized classifier. *Remote sensing of environment*, *219*, 180-195.

Porkka, M., Gerten, D., Schaphoff, S., Siebert, S., & Kummu, M. (2016). Causes and trends of water scarcity in food production. *Environmental Research Letters*, *11*(1), 015001.

QGIS Development Team (2019). QGIS Geographic Information System. Open Source Geospatial Foundation Project. http://qgis.osgeo.org (accessed on 8 September 2019).

Ramankutty, N., Mehrabi, Z., Waha, K., Jarvis, L., Kremen, C., Herrero, M., & Rieseberg, L. H. (2018). Trends in global agricultural land use: implications for environmental health and food security. *Annual review of plant biology*, *69*, 789-815.

Ray, D. K., & Foley, J. A. (2013). Increasing global crop harvest frequency: recent trends and future directions. *Environmental Research Letters*, *8*(4), 044041.

Ray, D. K., West, P. C., Clark, M., Gerber, J. S., Prishchepov, A. V., & Chatterjee, S. (2019). Climate change has likely already affected global food production. *PloS one*, *14*(5), e0217148.

Jägermeyr, J., Gerten, D., Heinke, J., Schaphoff, S., Kummu, M., & Lucht, W. (2015). Water savings potentials of irrigation systems: global simulation of processes and linkages. *Hydrology and Earth System Sciences*, *19*(7), 3073-3091.

Rosa, L., Rulli, M. C., Davis, K. F., Chiarelli, D. D., Passera, C., & D'Odorico, P. (2018). Closing the yield gap while ensuring water sustainability. *Environmental Research Letters*, *13*(10), 104002.

Rufin, P., Levers, C., Baumann, M., Jagermeyr, J., Krueger, T., Kuemmerle, T., & Hostert, P. (2018). Global-scale patterns and determinants of cropping frequency in irrigation dam command areas. *Global Environmental Change*, *50*, 110–122.

Rufin, P., Frantz, D., Ernst, S., Rabe, A., Griffiths, P., & Özdoğan, M. (2019). Mapping Cropping Practices on a National Scale Using Intra-Annual Landsat Time Series Binning. *Remote Sensing*, *11*(3), 232.

Rufin, P., Müller, D., Schwieder, M., Pflugmacher, D., Hostert, P. (in prep.). Mapping the extent and frequency of irrigated summer cropping in Southeastern Anatolia since 1990 using Landsat data.

Schmidt, G., Jenkerson, C. B., Masek, J., Vermote, E., & Gao, F. (2013). *Landsat ecosystem disturbance adaptive processing system (LEDAPS) algorithm description* (No. 2013-1057). US Geological Survey.

Schmidt, M., Pringle, M., Devadas, R., Denham, R., & Tindall, D. (2016). A framework for large-area mapping of past and present cropping activity using seasonal Landsat images and time series metrics. *Remote Sensing*, *8*(4), 312.

Schwieder, M., Leitão, P. J., da Cunha Bustamante, M. M., Ferreira, L. G., Rabe, A., & Hostert, P. (2016). Mapping Brazilian savanna vegetation gradients with Landsat time series. *International journal of applied earth observation and geoinformation*, *52*, 361-370.

Seager, S., Turner, E. L., Schafer, J., & Ford, E. B. (2005). Vegetation's red edge: a possible spectroscopic biosignature of extraterrestrial plants. *Astrobiology*, *5*(3), 372-390.

Senf, C., Leitão, P. J., Pflugmacher, D., van der Linden, S., & Hostert, P. (2015). Mapping land cover in complex Mediterranean landscapes using Landsat: Improved classification

accuracies from integrating multi-seasonal and synthetic imagery. *Remote Sensing of Environment*, *156*, 527-536.

Siebert, S., Henrich, V., Frenken, K., & Burke, J. (2013). Update of the digital global map of irrigation areas to version 5. *Rheinische Friedrich-Wilhelms-Universität, Bonn, Germany and Food and Agriculture Organization of the United Nations, Rome, Italy*.

Singh, A. (2016). Evaluating the effect of different management policies on the long-term sustainability of irrigated agriculture. *Land Use Policy*, *54*, 499-507.

Song, X. P., Potapov, P. V., Krylov, A., King, L., Di Bella, C. M., Hudson, A., Khan, A., Adusei, B., Stehamn, S. & Hansen, M. C. (2017). National-scale soybean mapping and area estimation in the United States using medium resolution satellite imagery and field survey. *Remote sensing of environment*, *190*, 383-395.

Stehman, S. V. (2001). Statistical rigor and practical utility in thematic map accuracy assessment. *Photogrammetric Engineering and Remote Sensing*, *67*(6), 727-734.

TARIM (2015). Crop calendar for Turkey. A compilation of planting and harvesting dates for selected Turkish provinces. *Turkish Ministry of Agriculture and Forestry.*

The R Project (2015). The R Foundation for Statistical Computing, Vienna, Austria.

Tilman, D., Balzer, C., Hill, J., & Befort, B. L. (2011). Global food demand and the sustainable intensification of agriculture. *Proceedings of the National Academy of Sciences*, *108*(50), 20260-20264.

TSI (2015). Turkish Statistical Institute. Crop Production Statistics. Agricultural Land. Available online: http://www.turkstat.gov.tr/ (accessed on 8 September 2019).

UN (2017). UN Department of Economic and Social Affairs. World population prospects, the 2017 Revision, Volume I: comprehensive tables. *New York United Nations Department of Economic & Social Affairs*.

USDA (2019). Turkey Cotton and Products Annual. Available online: https://gain.fas.usda.gov/Recent%20GAIN%20Publications/Cotton%20and%20Products%20Annual_Ankara_Turkey_3-29-2019.pdf (accessed on 8 September 2019).

USGS (2019a). Landsat Collections. https://www.usgs.gov/land-resources/nli/landsat/landsat-collections (accessed on 8 September 2019).

USGS (2019b). Landsat Collection 1. https://www.usgs.gov/land-resources/nli/landsat/landsat-collection-1 (accessed on 8 September 2019).

USGS (2019c). Landsat 4-7. surface reflectance (LEDAPS). Product guide. Version 2.0. Available online: https://prd-wret.s3-us-west-2.amazonaws.com/assets/palladium/production/atoms/files/LSDS-1370_L4-

7_Surface_Reflectance_LEDAPS_Product_Guide-v2.0.pdf (accessed on 8 September 2019).

USGS (2019d). Landsat 8. surface reflectance code (LaSRC). Product guide. Version 2.0. Available online: https://prd-wret.s3-us-west-2.amazonaws.com/assets/palladium/production/atoms/files/LSDS-1368_L8_Surface_Reflectance_Code_LASRC_Product_Guide-v2.0.pdf (accessed on 8 September 2019).

USGS (2019e). CFMask Algorithm. https://www.usgs.gov/land-resources/nli/landsat/cfmask-algorithm (accessed on 8 September 2019).

USGS (2019f). Landsat Collection 1 Level-1 Quality Assessment Band. https://www.usgs.gov/land-resources/nli/landsat/landsat-collection-1-level-1-quality-assessment-band (accessed on 8 September 2019).

USGS (2019g). Landsat 8. https://www.usgs.gov/land-resources/nli/landsat/landsat-8 (accessed on 8 September 2019).

USGS (2019h). Landsat 7. https://www.usgs.gov/land-resources/nli/landsat/landsat-7 (accessed on 8 September 2019).

Waldner, F., Hansen, M. C., Potapov, P. V., Löw, F., Newby, T., Ferreira, S., & Defourny, P. (2017). National-scale cropland mapping based on spectral-temporal features and outdated land cover information. *PloS one*, *12*(8), e0181911.

Whitcraft, A. K., Vermote, E. F., Becker-Reshef, I., & Justice, C. O. (2015). Cloud cover throughout the agricultural growing season: Impacts on passive optical earth observations. *Remote sensing of Environment*, *156*, 438-447.

Woodcock, C. E., Allen, R., Anderson, M., Belward, A., Bindschadler, R., Cohen, W., Gao, F., Goward, S. N., Helder, D., Helmer, E., Nemani, R., Oreopoulos, L., Schott, J., Thenkabail, P. S., Vermote, E. F., Vogelmann, J., Wulder, M. A. & Wynne, R. (2008). Free access to Landsat imagery. *Science*, *320*(5879), 1011-1011.

Wulder, M. A., White, J. C., Goward, S. N., Masek, J. G., Irons, J. R., Herold, M., Cohen, W. B., Loveland, T. R. & Woodcock, C. E. (2008). Landsat continuity: Issues and opportunities for land cover monitoring. *Remote Sensing of Environment*, *112*(3), 955-969.

Wulder, M. A., Masek, J. G., Cohen, W. B., Loveland, T. R., & Woodcock, C. E. (2012). Opening the archive: How free data has enabled the science and monitoring promise of Landsat. *Remote Sensing of Environment*, *122*, 2-10.

Wulder, M. A., & Coops, N. C. (2014). Satellites: Make Earth observations open access. *Nature News*, *513*(7516), 30.

WWF (2019). World Wildlife Fund. Terrestrial Ecoregions. https://www.worldwildlife.org/biome-categories/terrestrial-ecoregions (accessed on 8 September 2019).

Zabel, F., Delzeit, R., Schneider, J. M., Seppelt, R., Mauser, W., & Václavík, T. (2019). Global impacts of future cropland expansion and intensification on agricultural markets and biodiversity. *Nature communications*, *10*(1), 2844.

Zhu, Z., Wang, S., & Woodcock, C. E. (2015). Improvement and expansion of the Fmask algorithm: Cloud, cloud shadow, and snow detection for Landsats 4–7, 8, and Sentinel 2 images. *Remote Sensing of Environment*, *159*, 269-277.

Appendix

Appendix 1: Sample size calculation (Olofsson et al., 2014).

Stratified random					
Class	User's Accuracy	Pixel count	W - Mapped area proportion	S - Standard deviation	W*S
W & SC	0.90	17,653,692	0.203	0.3000	0.0610
Other	0.90	16,296,018	0.188	0.3000	0.0563
Other arable	0.90	15,518,517	0.179	0.3000	0.0536
Grassland	0.90	37,393,419	0.430	0.3000	0.1291
NoData		4,673			
SUM		86,866,319			
S(O)	0.01	Standard error of the estimated overall accuracy			
n	900	Number of reference samples			

Appendix 2: Classification frequency table & merged classes for strata.

Class	Value	Count	m^2	ha	km^2	%
Masked	0	4673	4205700	420.57	4.21	0.01
Water	1	1271921	1144728900	114472.89	1144.73	1.46
W & SC	2	17653692	1.5888E+10	1588832.28	15888.32	20.32
Grassland	3	37393419	3.3654E+10	3365407.71	33654.08	43.05
Urban/ open ?	4	13787268	1.2409E+10	1240854.12	12408.54	15.87
Forested	5	1236829	1113146100	111314.61	1113.15	1.42
Other arable	6	15518517	1.3967E+10	1396666.53	13966.67	17.86
	N/A	139242691				
	SUM	86866319	7.818E+10	7817968.71	78179.69	100
Class Acc_Ass						
W & SC		17653692				
Other arable		15518517				
Grassland		37393419				
Other		16296018				
Masked		4673				
	SUM	86866319				

Appendix 3: Sample allocation & invalid pixel information.

Sample allocation						
Class	Equal	Proportional	Invalid	no high-resolution	mixed-pixel	Invalid (%)
W & SC	225	183	18	3	15	9.841
Other	225	169	8	3	5	4.738
Other arable	225	161	6	1	5	3.732
Grassland	225	387	29	6	23	7.485
NoData						
SUM			61	13	48	6.778

Appendix 4: Overlay frequency table.

Pixel count	Adıyaman	Batman	Diyarbakır	Gaziantep	Kilis	Mardin	Şanlıurfa	Siirt	Şırnak	pixel SUM	km²
SC	143509	91804	744890	158976	21967	107296	2107373	43662	68614	3488091	3139.28
W & SC	1331277	795768	4619323	943608	223087	1418925	4794720	366951	561880	15055539	13549.99
Double	8318	11758	47553	79328	15731	891462	1279744	1667	79213	2414774	2173.30
Cropland SUM	1483104	899330	5411766	1181912	260785	2417683	8181837	412280	709707	20958404	18862.56
Area SUM	7738837	5056794	16616282	7393461	1529398	9563278	21386570	5995977	7932288	83212885	74891.60
W & SC in % of all cropland	89.76	88.48	85.36	79.84	85.54	58.69	58.60	89.01	79.17		
Double in % of all cropland	0.56	1.31	0.88	6.71	6.03	36.87	15.64	0.40	11.16		
Cropland in % of total province are	19.16	17.78	32.57	15.99	17.05	25.28	38.26	6.88	8.95		
Hectares (ha)	Adıyaman	Batman	Diyarbakır	Gaziantep	Kilis	Mardin	Şanlıurfa	Siirt	Şırnak	ha SUM	km²
Winter & spring crops	119814.93	71619.12	415739.07	84924.72	20077.83	127703.25	431524.80	33025.59	50569.20	1354998.51	13549.99
Summer crops	12915.81	8262.36	67040.10	14307.84	1977.03	9656.64	189663.57	3929.58	6175.26	313928.19	3139.28
Double cropping	748.62	1058.22	4279.77	7139.52	1415.79	80231.58	115176.96	150.03	7129.17	217329.66	2173.30
area sum	696495.33	455111.46	1495465.38	665411.49	137645.82	860695.02	1924791.30	539637.93	713905.92	7489159.65	74891.60
all cropland sum	133479.36	80939.70	487058.94	106372.08	23470.65	217591.47	736365.33	37105.20	63873.63	1886256.36	18862.56

Appendix 5: Accuracy statistics (area-adjusted calc.) for the first classification

Accuracy statistics (area-adjusted calculation)						Overall accuracy		Producer's Accuracy 95% CI	User's Accuracy 95% CI	Overall Accuracy 95% CI
	Producer's Accuracy	User's Accuracy	Omission Error	Commission Error						
other arable	49.27%	64.96%	50.73%	35.04%				5.92%	8.68%	
WC	90.83%	82.82%	9.17%	17.18%				3.71%	4.92%	
other	78.94%	75.68%	21.06%	24.32%				5.96%	6.94%	
grassland	85.14%	82.84%	14.86%	17.16%		79.34%		3.02%	3.66%	2.62%

Appendix 6: Visible SLC failure influence on classification (WC_val_sample_NEW, cell#50872646).
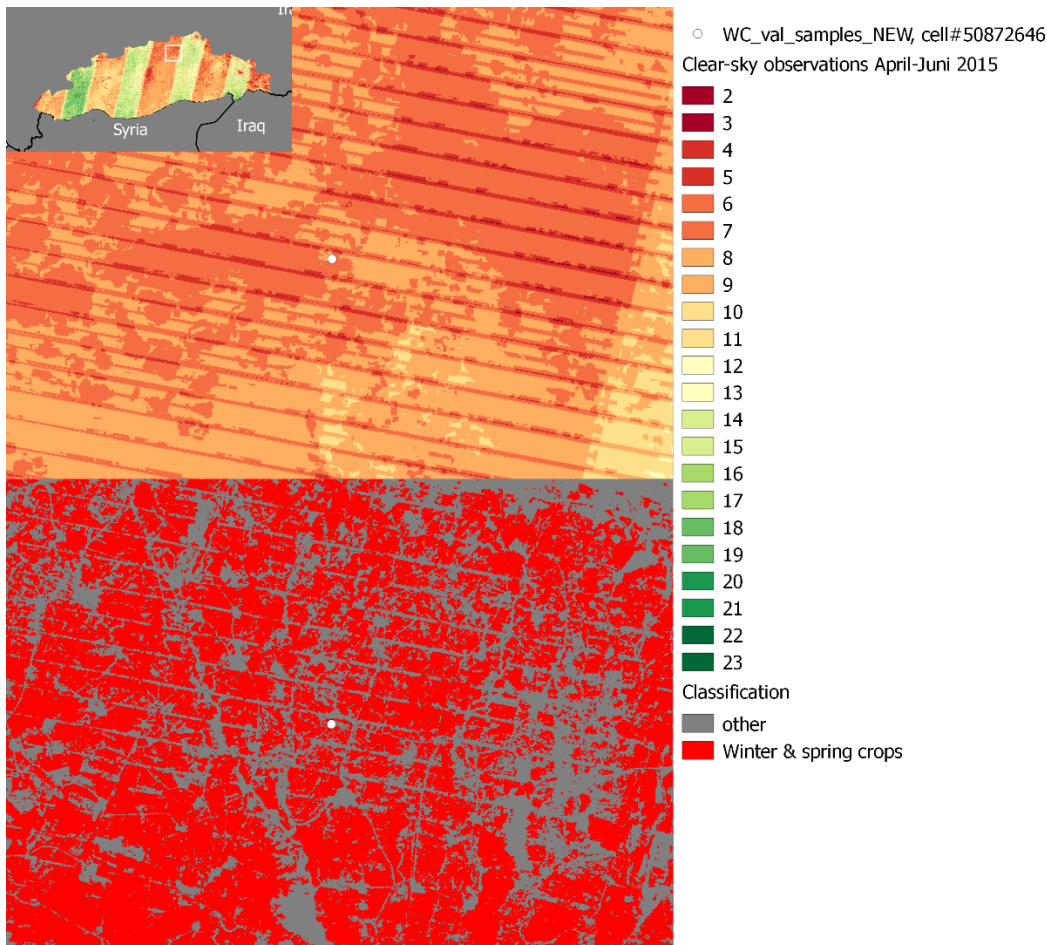
ERKLÄRUNG

Ich erkläre, dass ich die vorliegende Arbeit nicht für andere Prüfungen eingereicht, selbständig und nur unter Verwendung der angegebenen Literatur und Hilfsmittel angefertigt habe. Sämtliche fremde Quellen inklusive Internetquellen, Grafiken, Tabellen und Bilder, die ich unverändert oder abgewandelt wiedergegeben habe, habe ich als solche kenntlich gemacht. Mir ist bekannt, dass Verstöße gegen diese Grundsätze als Täuschungsversuch bzw. Täuschung geahndet werden.

Berlin, den 10. September 2019

Unterschrift